JOURNAL OF VIROLOGY, Sept. 2009, p. 9432–9448 Vol. 83, No. 18
0022-538X/09/$08.00+0 doi:10.1128/JVI.00739-09

Subcellular Localization of the *Barley Stripe Mosaic Virus* Triple Gene Block Proteins[▽]

Hyoun-Sub Lim,[1,2] Jennifer N. Bragg,[1] Uma Ganesan,[1] Steven Ruzin,[1] Denise Schichnes,[1] Mi Yeon Lee,[1,4] Anna Maria Vaira,[2,3] Ki Hyun Ryu,[4] John Hammond,[2] and Andrew O. Jackson[1]*

Department of Plant and Microbial Biology, University of California, Berkeley, California 94720[1]; FNPRU, Agricultural Research Service, U.S. Department of Agriculture, Beltsville, Maryland 20705[2]; CNR, Istituto di Virologia Vegetale, Torino 10135, Italy[3]; and Plant Virus GenBank, Division of Environmental and Life Sciences, Seoul Women's University, Seoul 139-774, South Korea[4]

Received 9 April 2009/Accepted 22 June 2009

Barley stripe mosaic virus **(BSMV) spreads from cell to cell through the coordinated actions of three triple gene block (TGB) proteins (TGB1, TGB2, and TGB3) arranged in overlapping open reading frames (ORFs). Our previous studies (D. M. Lawrence and A. O. Jackson, J. Virol. 75:8712-8723, 2001; D. M. Lawrence and A. O. Jackson, Mol. Plant Pathol. 2:65-75, 2001) have shown that each of these proteins is required for cell-to-cell movement in monocot and dicot hosts. We recently found (H.-S. Lim, J. N. Bragg, U. Ganesan, D. M. Lawrence, J. Yu, M. Isogai, J. Hammond, and A. O. Jackson, J. Virol. 82:4991-5006, 2008) that TGB1 engages in homologous interactions leading to the formation of a ribonucleoprotein complex containing viral genomic and messenger RNAs, and we have also demonstrated that TGB3 functions in heterologous interactions with TGB1 and TGB2. We have now used *Agrobacterium tumefaciens*-mediated protein expression in *Nicotiana benthamiana* leaf cells and site-specific mutagenesis to determine how TGB protein interactions influence their subcellular localization and virus spread. Confocal microscopy revealed that the TGB3 protein localizes at the cell wall (CW) in close association with plasmodesmata and that the deletion or mutagenesis of a single amino acid at the immediate C terminus can affect CW targeting. TGB3 also directed the localization of TGB2 from the endoplasmic reticulum to the CW, and this targeting was shown to be dependent on interactions between the TGB2 and TGB3 proteins. The optimal localization of the TGB1 protein at the CW also required TGB2 and TGB3 interactions, but in this context, site-specific TGB1 helicase motif mutants varied in their localization patterns. The results suggest that the ability of TGB1 to engage in homologous binding interactions is not essential for targeting to the CW. However, the relative expression levels of TGB2 and TGB3 influenced the cytosolic and CW distributions of TGB1 and TGB2. Moreover, in both cases, localization at the CW was optimal at the 10:1 TGB2-to-TGB3 ratios occurring in virus infections, and mutations reducing CW localization had corresponding effects on BSMV movement phenotypes. These data support a model whereby TGB protein interactions function in the subcellular targeting of movement protein complexes and the ability of BSMV to move from cell to cell.**

Plants use macromolecular trafficking pathways through plasmodesmata (PD) as a means to regulate developmental processes and physiological functions, and they also rely on these channels as avenues to communicate and mount defense responses to pathogen challenge (2, 37, 55). Local and systemic plant virus invasion depends on the abilities of viruses to use these pathways to spread from initially infected cells to the vascular tissue and distal regions of the plant. To this end, viruses infecting plants have evolved movement proteins (MPs) that coopt host trafficking pathways to target virus genomes to the PD and to facilitate the cell-to-cell transit of infectious entities (4, 13, 36, 48, 55). Virus MPs vary in size, number, and genome organization, but they share a number of functional characteristics including localization to PD, an ability to increase the size exclusion limits of PD, and RNA binding activities (3, 7, 8, 24, 27, 58).

Viruses containing triple gene block (TGB) MPs have been the subjects of a number of investigations (4, 6, 39, 53, 54). Interestingly, viruses with a range of diverse genome structures encode MPs in a TGB, but these proteins fall into two major TGB classes that have substantial differences in protein structure and variations in their physical, functional, and cellular interactions (19, 30, 39, 45, 48). For example, the hordeivirus-like TGB1 proteins contain substantial N-terminal extensions that are lacking in the potexvirus-like TGB1 proteins, but the two classes of proteins share a conserved helicase domain at their C termini (39). The available evidence also indicates that hordeivirus-like and potexvirus-like TGB1 proteins share common biochemical features, including RNA binding abilities (3, 13, 23, 35, 44, 56), RNA helicase activities (22), associated NTPase activities (3, 13, 23, 33, 35, 44), and the capacity to form homologous interactions (29, 30, 45). However, the potexvirus-like TGB1 proteins localize at the CW when expressed autonomously and also facilitate increases in PD size exclusion limits, whereas the hordeivirus-like TGB1 proteins lack both

* Corresponding author. Mailing address: Department of Plant and Microbial Biology, University of California, 111 Koshland Hall, Berkeley, CA 94720. Phone: (510) 642-3906. Fax: (510) 642-4995. E-mail: andyoj@berkeley.edu.

▽ Published ahead of print on 1 July 2009.

these activities (39, 53). Major differences are also evident in the organizations of the potexvirus-like and hordeivirus-like TGB3 proteins, which share no discernible relatedness, differ in the numbers of their transmembrane domains, and indeed appear to have a polyphyletic origin (39).

In both TGB classes, the movement strategy employs the coordinated actions of all three proteins. However, the coat protein is dispensable for one or more phases of movement of benyvirus, hordeivirus, pecluvirus, and pomovirus, encoding hordeivirus-like (class I) MPs, but is absolutely required for cell-to-cell movement of potexvirus-like (class II) MPs encoded by allexivirus, carlavirus, foveavirus, and potexvirus (6, 19, 39, 54). These variations clearly demonstrate that the two classes of TGB proteins have profound differences in their functional properties and in their associations with other virus and host proteins. Hence, comparative analyses of the functional and biological properties of the two classes of proteins in their common hosts may reveal important activities relevant to viral pathogenesis. To provide more information about the hordeivirus-like movement mechanisms, we are investigating the TGB interactions of *Barley stripe mosaic virus* (BSMV).

BSMV is the type member of the genus *Hordeivirus*, which includes *Poa semilatent virus* (PSLV), *Lychnis ringspot virus*, and *Anthoxanthum latent blanching virus* (6, 19). Hordeiviruses have positive-sense, single-stranded RNA genomes consisting of three segments, designated α, β, and γ. The RNAβ segment encodes the coat protein, which is translated directly from genomic RNAβ (gRNAβ), and the TGB proteins, which are expressed from two subgenomic RNAs (sgRNAs), designated sgRNAβ1 and sgRNAβ2 (60). The coat protein is dispensable for the systemic movement of BSMV (41), and mutational analyses indicate that the TGB1, TGB2, and TGB3 proteins are each essential for cell-to-cell movement in monocot and dicot hosts (28). The BSMV TGB1 (58-kDa) protein is expressed from sgRNAβ1 at higher levels than the smaller hydrophobic TGB2 (14-kDa) and TGB3 (17-kDa) proteins, which are coexpressed from the bicistronic sgRNAβ2 during replication (14, 60). BSMV TGB1 has binding activity for both single-stranded and double-stranded RNAs (13) and forms nucleoprotein complexes with each of the BSMV gRNAs and sgRNAs (30). The hordeivirus-like TGB1 proteins differ from the potexvirus-like TGB1 proteins in having longer N-terminal domains with positively charged amino acids, but both classes of proteins have conserved C-terminal NTPase/helicase domains (13, 39, 49). In BSMV, mutations of conserved amino acids within the TGB1 helicase motif abrogate cell-to-cell movement and alter subcellular localization in infected protoplasts (27). Plants infected with a BSMV β-green fluorescent protein-TGB1 (β-GFP-TGB1) reporter virus also exhibited paired foci on both sides of the CW, and the plasma membranes of infected protoplasts developed punctate foci (27). TGB1 and TGB2 are also essential for plasma membrane targeting because β-GFP-TGB1 reporter derivatives that were unable to express TGB2 or TGB3 fluoresce at perinuclear membranes of protoplasts (27). Particle bombardment studies with the related hordeivirus PSLV also suggested that the expression of TGB3 is required to shift the localization of TGB2 from the endoplasmic reticulum (ER) to the peripheral membranes (50), and transgenically expressed PSLV TGB3 appears to be associated with PD due to its colocalization with callose markers (17).

We have recently shown that TGB2 and TGB3 interact physically and have identified single amino acids in each protein that are required for these interactions (19, 30). TGB3 also interacts with TGB1, and we have proposed that these interactions facilitate the transport of ribonucleoprotein (RNP) complexes to the PD (30). However, the effects of TGB protein interactions on subcellular localization have not been defined. Moreover, because of possible convergent evolution of the hordeivirus-like and potexvirus-like TGB-containing viruses (39), the mechanisms of action resulting in transport may differ among different genera or even among different virus species within a genus. To obtain more refined information about these processes, we have now expressed fluorescent TGB fusion proteins transiently in *Nicotiana benthamiana* leaf cells by *Agrobacterium tumefaciens* infiltration and have assessed the subcellular localization patterns of BSMV wild-type (wt) and mutant TGB derivatives that differ in their interactions. We also have carried out reverse genetic experiments with selected BSMV TGB mutants to provide a biological context for the localization patterns appearing during ectopic *Agrobacterium* expression. These findings are elaborated in a model for TGB interactions required for the cell-to-cell movement of BSMV.

MATERIALS AND METHODS

***Agrobacterium* infiltration and BSMV cDNA constructs.** All binary vectors used in these studies were derived from pGD plasmids (pGD, pGDG, and pGDR), each of which contains a single 35S promoter to drive transcription (16). Oligonucleotides used in cloning and sequencing are summarized in Table 1 and were described previously by Lim et al. (30). A GFP-talin actin marker (25), obtained from Nam-Hai Chua (Rockefeller University), was amplified using the primers indicated in Table 1. The PCR product was digested with XhoI and SalI and ligated into the corresponding sites in pGDR or pGDG *Agrobacterium tumefaciens* expression vectors (16). Plasmid pTMV-ROPL was obtained from Patricia Zambryski (University of California, Berkeley) for the recovery of tobacco mosaic virus (TMV) P30-GFP as a PD marker (10, 12, 52). The P30-GFP sequence was excised by XhoI and PstI digestion and ligated into the corresponding sites of the pGD vector (16). A transgenic *N. benthamiana* line expressing the GFP-KDEL ER marker was provided by David Baulcombe (John Innes Centre, Norwich, United Kingdom).

Plasmids were designed for the individual expression of TGB1, TGB2, or TGB3, and fluorescent fusion proteins were constructed for each TGB protein by amplification from the BSMV β42SpI cDNA clone (43) using the primers indicated in Table 1. A plasmid, pTGB2/3, capable of expressing a single mRNA analogous to sgRNAβ2 (60) was also engineered for the expression of ~10:1 ratios of TGB2 and TGB3. Mutant derivatives of TGB1, TGB2, TGB3, and TGB2/3 were generated using a modified overlap extension PCR method (57). wt and mutant TGB derivatives were inserted into the XhoI and BamHI sites of the pGD vector (16) to generate the clones unique to our experiments. The cloning mechanisms and primers used for mutagenesis are listed in Table 1.

Agrobacterium infiltrations of *N. benthamiana* leaves were performed essentially as described previously by Johansen and Carrington (20), with minor modifications which we implemented as described previously (5, 11, 16). In preparation for agroinfiltration, cultures were mixed in the desired combinations to a final concentration of 0.6 to 0.8 A_{600} units per ml and usually included bacteria containing plasmid pGD:γb to minimize host gene silencing (5). Control experiments indicated that the presence of γb increased the duration of fluorescence but did not affect the subcellular distribution of the proteins. Mixtures were incubated at room temperature for 2 to 3 h before pressure infiltration into the leaves with a 1-ml syringe.

Plasmolysis was usually induced at 36 h after agroinfiltration by pressure infiltrating leaves with 700 mM sucrose, followed by soaking the leaves in sucrose solution for 6 to 8 h. For CW staining experiments, 70 μg/ml of calcofluor blue

TABLE 1. Clones and oligonucleotides used in localization, infectivity, and real-time quantitative PCR experiments

Clone	5′ oligonucleotide	5′ oligonucleotide sequence	3′ oligonucleotide	3′ oligonucleotide sequence	Change and/or reference or source[a]
pGD constructs used in *Agrobacterium* infiltration experiments					
pGDG:TGB1	TGB1 XhoIF	GACTCGAGCCATGGACATGACGAAAACT	TGB1 BamHIR	TAGGATCCTTATTTGGCCTTGAACCAACTGTG	wt
pGDG:TGB2	TGB2 XhoIF	GCCTCGAGGGATGAAGACCACAGTTGG	TGB2 BamHIR	TAGGATCCCTAGCCAATATCGCATAGTAATG	wt
pGDG:TGB3 and pGDR:TGB3	TGB3 XhoIF	CCCTCGAGCTATGGCAATGCCTCATCCC	TGB3 BamHIR	TTGGATCCTTACCTTTTTGAAGAAAGTA AGAG	wt
pGD:TGB3$_{16\text{-}155}$	TGB3 XhoIF	CCCTCGAGCTATGCCATCGGATCATT	TGB3 BamHIR	TTGGATCCTTACCTTTTTGAAGAAAGTA AGAG	Delete aa 1-15
pGDR:TGB3$_{16\text{-}155}$	N delete XhoIF	GAGCTCGAGAAATGACCGTGCTCGCTTGCA	TGB3 BamHIR	TTGGATCCTTACCTTTTTGAAGAAAGTA AGAG	Delete aa 1-15
pGDR:TGB3$_{1\text{-}150}$	TGB3 XhoIF	CCCTCGAGCTATGGCAATGCCTCATCCC	C delete BamHIR	TTGGATCCTTAGAGAAAAAAGCTTAACGC AAAA	Delete aa 151-155
pGDR:TGB3$_{154}$	TGB3 XhoIF	CCCTCGAGCTATGGCAATGCCTCATCCC	BamHI$_{154}$ R	TTGGATCCTTATTTTGAAGAAAGTAAGAGAA AAAA	Delete R155
pGDR:TGB3$_{153}$	TGB3 XhoIF	CCCTCGAGCTATGGCAATGCCTCATCCC	BamHI$_{153}$ R	TTGGATCCTTATGAAGAAAGTAAGAGAAA AAG	Delete K154 and R155
pGDR:TGB3$_{R155A}$	TGB3 XhoIF	CCCTCGAGCTATGGCAATGCCTCATCCC	BamHI$_{R155A}$ R	TTGGATCCTTATGCTTTTGAAGAAAGTAAGA GAAAAAA	Substitute R155A
pGDR:TGB3$_{K154A}$	TGB3 XhoIF	CCCTCGAGCTATGGCAATGCCTCATCCC	BamHI$_{K154A}$ R	TTGGATCCTTACCTTGCTGAAGAAAGTAAGA GAAAAAA	Substitute K154A
pGDR:TGB3$_{K154A,R155A}$	TGB3 XhoIF	CCCTCGAGCTATGGCAATGCCTCATCCC	BamHI$_{K154A,R155A}$ R	TTGGATCCTTATGCCGCTGAAGAAAGTAAGA GAAAAAAG	Substitute K154A and R155A
pGDG:Talin and pGDR:Talin	Talin XhoF	TTCTCGAGCTATGATCCTAGAAGCTGCCAA GTCCATCGCTGCAGC	Talin SalR	TTGTCGACTTAGTGCTCGTCTCGAAGCTCTGA AGGCA	
pGD:TGB2/3	TGB2 XhoIF	GCCTCGAGGGATGAAGACCACAGTTGG	TGB3 BamHIR	TTGGATCCTTACCTTTTTGAAGAAAGTA AGAG	
pGD:TGB2$_{G40R,D41R}$/3	TGB2 XhoIF	GCCTCGAGGGATGAAGACCACAGTTGG	TGB3 BamHIR	TTGGATCCTTACCTTTTTGAAGAAAGTA AGAG	Substitute TGB2 G40R and D41R; 30
pGD:TGB2/3$_{P105R,I108R}$	TGB2 XhoIF	GCCTCGAGGGATGAAGACCACAGTTGG	TGB3 BamHIR	TTGGATCCTTACCTTTTTGAAGAAAGTA AGAG	Substitute TGB3 P105R and I108R; 30
pGD:TGB2/3$_{1\text{-}150}$	TGB2 XhoIF	GCCTCGAGGGATGAAGACCACAGTTGG	TGB3 BamHIR	TTGGATCCTTAGAGAAAAAAGCTTAACGC AAAA	Delete aa 151-155
pGD:TMV:MP:GFP					pTMV-ROPL XhoI and PstI fragment inserted into pGD
BSMV derivatives used in infectivity experiments					
BSMVβ-GFP-TGB1					27
BSMVβ-GFP-TGB1/TGB3$_{153}$	Pst Forward	GATGACCTGTTGCTTTCTGCAGTTCCGATA ACGTCT	SpeI R	GAGACTAGTTGGTCTTCCCTTGGGGGACC GAAG	Delete K154 and R155
	TGB3$_{153}$ F	TTTTCTCTTACTTTCTTCATAA	TGB3$_{153}$ R	TTATGAAGAAAGTAAGAGAAAA	
BSMVβ-GFP-TGB1/TGB3$_{154}$	Pst Forward	GATGACCTGTTGCTTTCTGCAGTTCCGATA ACGTCT	SpeI R	GAGACTAGTTGGTCTTCCCTTGGGGGACC GAAG	Delete R155
	TGB3$_{154}$ F	TTTTCTCTTACTTTCTTCAAAATAA	TGB3$_{154}$ R	TTATTTTGAAGAAAGTAAGAGAAAA	
BSMVβ-GFP-TGB1/TGB3$_{K154A,R155A}$	Pst Forward	GATGACCTGTTGCTTTCTGCAGTTCCGATA ACGTCT	SpeI R	GAGACTAGTTGGTCTTCCCTTGGGGGACC GAAG	Substitute K154A and R155A
	TGB3$_{K154A,R155A}$F	TCTCTTACTTTCTTCAGCAGCCTAA	TGB3$_{K154A,R155A}$R	TTAGGCTGCTGAAGAAAGTAAGAGA	
BSMVβ-GFP-TGB1/TGB3$_{R155A}$	Pst Forward	GATGACCTGTTGCTTTCTGCAGTTCCGATA ACGTCT	SpeI R	GAGACTAGTTGGTCTTCCCTTGGGGGACC GAAG	
	TGB3$_{R155A}$F	TCTCTTACTTTCTTCAAAAGCCTAA	TGB3$_{R155A}$R	TTAGGCTTTTGAAGAAAGTAAGAGA	Substitute R155A
BSMVβ-GFP-TGB1/TGB3$_{1\text{-}150}$	Pst Forward	GATGACCTGTTGCTTTCTGCAGTTCCGATA ACGTCT	SpeI R	GAGACTAGTTGGTCTTCCCTTGGGGGACC GAAG	Delete aa 151-155 (LSSKR)
	TGB3$_{1\text{-}150}$F	TGATAGCTAACTGAAAAAAAAAAAAAAAA AAAA	TGB3$_{1\text{-}150}$R	TCAGTTAGCTATCAAAGAGAAAAAAGCTT	
BSMVβ-GFP-TGB1/TGB2$_{G40R,P41R}$				SpeI/PstI fragment from BSMVβ-TGB2$_{G40R,D41R}$ inserted into BSMVβ-GFP-TGB1	30
BSMVβ-GFP-TGB1/TGB3$_{P105R,I108R}$				SpeI/PstI fragment from BSMVβ-TGB3$_{P105R,I108R}$ inserted into BSMVβ-GFP-TGB1	30
Primers used in real-time quantitative PCR experiments					
TGB1	TGB1 F	CCGGTGATCTACAGATCAGAGA	TGB1 R	AATTGCCAGGGCACAATCGTACC	BSMVβ nt 1875-2093
TGB2	TGB2 F	ATGAAGACCACAGTTGG	TGB2 R	GGCAAAAGGATGATTACG	BSMVβ nt 2311-2514
TGB3	TGB3 F	TATCAAGATCTGAACTCTGT	TGB3 R	CCTTTTTGAAGAAAGTAAGAG	BSMVβ nt 2780-2980
N. benthamiana Actin	Actin F	AAGACCAGCTCATCCGTGGA	Actin R	CTCATCCTATCAGCAATGCCC	GenBank accession no. AY179605

[a] aa, amino acids; nt, nucleotides.

TABLE 2. Quantitative PCR transcript levels in *N. benthamiana* leaf tissue infiltrated with constant TGB1 and various ratios of TGB2 to TGB3 in *Agrobacterium* cultures

Agrobacterium culture ratio (TGB2 to TGB3)[a]	Amt of inoculum (μl)				No. of plants	Mean relative TGB2/TGB3 quantitative PCR transcript level ± SD[c]
	pGDG:TGB1[b]	pGD:TGB2	pGD:TGB3	pGD		
10:1	500	400	40	60	5	7.5 ± 1.9
1:1	500	220	220	60	4	1.3 ± 1.0
1:10	500	40	400	60	4	0.1 ± 0.1

[a] All cultures have an optical density at 600 nm of 0.6.
[b] GFP-TGB1 transcript level relative to that of actin: ΔC_T(GFP-TGB1 − actin) = 6.86 ± 1.82.
[c] $2^{-\Delta\Delta CT} = 2^{-[\Delta CT(TGB2\text{-}actin) - \Delta CT(TGB3\text{-}actin)]}$.

(Sigma-Aldrich Chemical, St. Louis, MO) was added to 700 mM sucrose and infiltrated 30 min before microscopy.

BSMV infectivity and GFP-TGB1 subcellular localization experiments. Full-length infectious cDNA transcripts corresponding to RNAs α, β, and γ of BSMV strain ND18 were prepared as previously described (42). In order to assess the effects of TGB2 and TGB3 mutations on movement in inoculated plants, BSMV RNAγ-γb-GFP (28) or BSMV RNAβ GFP-TGB1 mutant reporter derivatives (27) were substituted for wt RNAγ or RNAβ in the inocula. The RNAβ-GFP-TGB1 reporter plasmid was also used as a background plasmid for the insertion of the TGB2-β$TGB2_{G40R,D41R}$/3 and TGB2/$3_{P105R,I108R}$ mutants constructed previously (30). These mutants were produced by linearizing and cutting RNAβ-GFP-TGB at the PstI (position 1710, corresponding to the BSMV RNAβ sequence) and the SpeI (position 3215) sites and then replacing the excised fragments with the analogous PstI and SpeI fragments generated from pDBDU: $TGB2_{G40R,D41R}$ or pDBDUTG$B3_{P105R,I108R}$ (30). The TGB3 C-terminal deletion mutants (β$TGB3_{153}$, β$TGB3_{154}$, β$TGB3_{K154A,R155A}$, and β$TGB3_{R155A}$) were produced by overlap PCR amplification of the PstI and SpeI fragments from the appropriate mutant plasmids (Table 1) and substitution of the resulting fragments into the PstI and SpeI sites of RNAβ-GFP-TGB1.

BSMV RNAs used in these experiments were transcribed individually in 50-μl transcription reaction mixtures containing 2 μg of linearized template DNA (42). After transcription, the gRNAs were pooled, precipitated with ethanol, resuspended in 20 μl of GKP buffer (50 mM glycine, 30 mM $KHPO_4$ [pH 9.2], 1% bentonite, 1% celite), and used to inoculate *N. benthamiana* leaves. The inoculated plants were maintained in plant growth chambers at 22°C with a 16-h light/8-h dark regimen under a light intensity of 120 $\mu mol \cdot m^{-2} \cdot s^{-1}$, which was produced by halogen lamps. Inoculated leaf sections were examined with a Zeiss LSM 410 or LSM 510 confocal microscope at 7 and 10 days after inoculation to assess the effects of the mutations on the spread of the virus.

Experiments to determine the effects of TGB2 and TGB3 mutations on the subcellular localization of GFP-TGB1 were conducted by inoculating wt RNAs α and γ in mixtures containing RNAβ-GFP-TGB1 derivatives. Control inocula containing wt RNAβ-GFP-TGB1 transcripts were used in some localization experiments. Inocula used to determine the effects of TGB2 and TGB3 mutations on GFP-TGB1 localization contained RNAβ-GFP-TGB1 mutants harboring site-specific substitutions that affect the heterologous interactions of TGB2 and TGB3 or site-specific and deletion mutations that interfere with CW targeting of TGB3. The transcript mixtures were inoculated into *N. benthamiana* plants, which were maintained in a growth chamber as described above. At 7 days postinfection (dpi), leaves were infiltrated with an *Agrobacterium* strain containing the DsRed-talin plasmid for use as a membrane marker. Leaf sections to be plasmolyzed were excised at 9 dpi and infiltrated with 700 mM sucrose for 6 h. Unplasmolyzed and plasmolyzed leaf sections were then examined by confocal fluorescence microscopy to evaluate the subcellular localization of GFP-TGB1.

Fluorescence assays. Fluorescence in epidermal cells of *N. benthamiana* leaves was visualized by confocal laser scanning microscopy using a Zeiss (Thornwood, NY) LSM 510 Meta microscope. GFP was excited using the 488-nm line of an argon laser and detected through a BP505-530 emission filter to the photomultiplier tube detector. DsRed was excited using an HeNe 543-nm laser and imaged using the Meta detector set for 570 to 600 nm. Images were acquired with a Zeiss LSM V3.2 Sp2 microscope, processed using Adobe Photoshop CS3 (Adobe Systems Inc., San Jose, CA), and presented as single optical sections. An Enterprise UV laser emitting at 358 and 364 nm was used to visualize calcofluor white-stained walls by the capture of emission spectra between 375 and 450 nm, and the resulting fluorescence was digitally manipulated to appear white.

QPCR analyses. All three TGB proteins were coexpressed in *N. benthamiana* leaves. The concentration (A_{600} = 0.6) of *Agrobacterium* cells containing the TGB1 expression plasmid was kept constant within treatments, and various amounts of bacteria containing the TGB2 or TGB3 expression plasmids were added to each infiltration mixture (Table 2). Each bacterial combination was repeated by infiltrating four to five individual plants. For real-time quantitative PCR analyses, leaf samples were examined by confocal laser scanning microscopy to evaluate the subcellular localization of the fluorescent fusion proteins prior to RNA extraction at 2 dpi. In order to measure GFP/TGB1, GFP/TGB2, and GFP/TGB3 mRNA expression ratios, 50 mg of infiltrated leaf tissue was ground to a fine powder in liquid nitrogen, and total RNA isolated using the RNeasy minikit (Qiagen, Valencia, CA) was treated with DNase I according to the manufacturer's recommendations. Total RNA (2 μg) was used to generate cDNA using the SuperScript III RNase H^- reverse transcriptase system (Invitrogen, Carlsbad, CA) in conjunction with an oligo$(dT)_{20}$ primer. Quantum PCRs (QPCRs) were performed with selected primer sets (Table 1) using the 7900HT sequence detection QPCR system (Applied Biosystems, New York, NY) and Brilliant SYBR green QPCR master mix (Stratagene, La Jolla, CA) as described previously by Bae et al. (1). A 25-μl QPCR reaction mixture contained 12.5 μl of 2× Brilliant SYBR green QPCR master mix, 5 μl of 10-fold-diluted cDNA, 2,500 nM of each gene-specific primer, and a diluted reference dye (final concentration of 300 nM). The amplification conditions used for the QPCR reactions were 95°C for 10 min and 40 cycles of 95°C for 30 s, 58°C for 1 min, and 72°C for 30 s. The ratios of the transcript levels of each TGB mRNA were calculated at 2 days after infiltration by comparison with an *ACTIN* (GenBank accession no. AY179605) mRNA that is constitutively expressed in *N. benthamiana* leaves (34), and the ratios were normalized using the real-time quantitative PCR $2^{-\Delta\Delta CT}$ method (34).

RESULTS

C-terminal residues are critical for targeting of TGB3 to the CW. Information about the subcellular localization of the BSMV TGB3 protein is not available in the context of a viral infection because of its low abundance in infected plants and our inability to raise antibodies to purified protein (14, 27). Therefore, in the experiments described below, DsRed-TGB3 or GFP-TGB3 and other proteins were coexpressed ectopically from *Agrobacterium* in infiltrated leaves, and at 2 to 3 days after infiltration, GFP localization was evaluated by differential interference contrast (DIC) or confocal laser scanning microscopy. Western blot analyses of tissues expressing GFP-TGB fusions with a GFP-specific antibody showed that all three proteins were present in coinfiltrated tissue and that these proteins migrated primarily in the monomeric form, with minimal aggregation or breakdown products being evident (data not shown). Our previous studies have shown that multiple proteins are expressed in more than 95% of the cells within an infiltrated region (11, 16), so it is likely that most cells contain the coexpressed proteins.

DIC microscopy of agroinfiltrated epidermal cells expressing the DsRed-TGB3 fusion protein revealed numerous pairs of bodies on opposite sides of the CW in patterns that appeared to coincide with the PD (Fig. 1A). To provide additional evidence to distinguish the localization of TGB3, bacteria harbor-

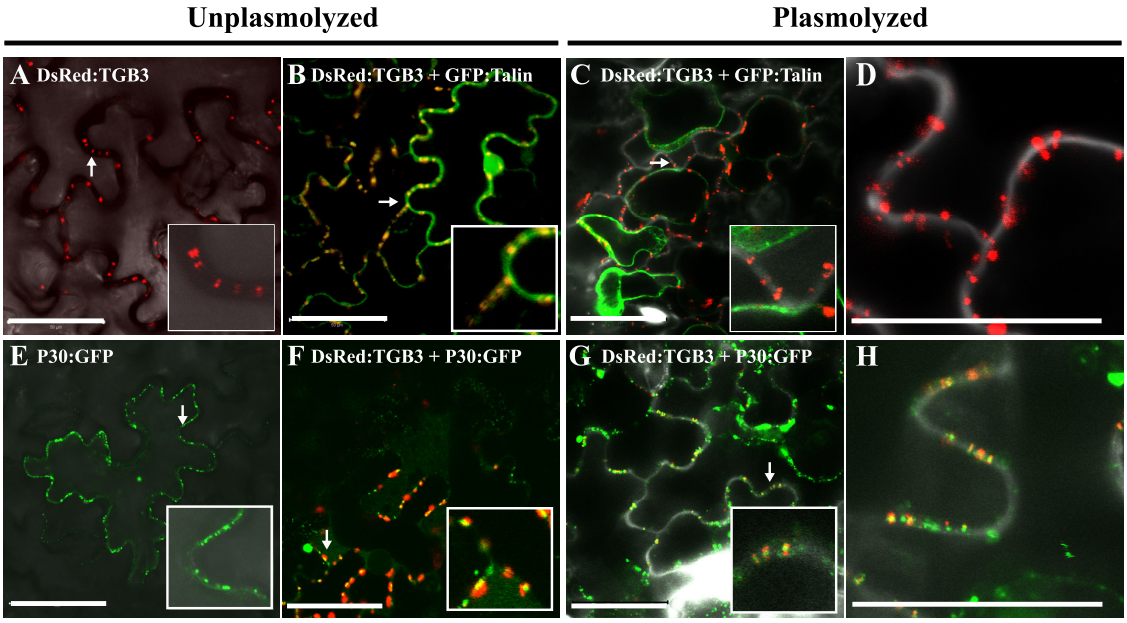

FIG. 1. Analysis of DsRed-TGB3 localization in agroinfiltrated *N. benthamiana* leaf cells. (A) Paired fluorescent foci of DsRed-TGB3 in unplasmolyzed epidermal leaf cells. (B) Cells coexpressing DsRed-TGB3 and GFP-talin as a cell membrane marker. (C) Fluorescence of DsRed-TGB3 in plasmolyzed leaf tissue containing GFP-talin. (D) Magnified image of DsRed-TGB3 in plasmolyzed tissue. (E) Tissue infiltrated with bacteria harboring the TMV P30-GFP (P30:GFP) plasmid to serve as a CW marker. (F) DsRed-TGB3 and TMV P30-GFP fluorescence in cells. (G and H) DsRed-TGB3 and P30-GFP coexpression in plasmolyzed leaf tissue. Note that plasmids were expressed in *N. benthamiana* leaves via agroinfiltration, and laser scanning confocal microscopy images of epidermal leaf cells were captured at 2 to 3 days after infiltration. Plasmolysis was carried out by infiltrating leaf sections with 700 mM sucrose before microscopic examination of tissue, and calcofluor blue CW staining was digitally manipulated to appear white. Arrows in the images identify the locations of magnified inset panels that highlight protein localization. Bars, 50 μm.

ing DsRed-TGB3 and the actin marker GFP-talin were mixed and infiltrated into leaf cells (Fig. 1B and C). The results for unplasmolyzed cells show that DsRed-TGB3 formed punctate spots at the CW but that GFP-talin generally fluoresced throughout the cytosol compartment (Fig. 1B). Moreover, when the infiltrated leaf sections were plasmolyzed, DsRed-TGB3 remained at the calcofluor-stained CW (note that the calcofluor fluorescence was digitally manipulated to appear white), whereas the GFP-talin-labeled cytoplasm detached from the CW (Fig. 1C and D; note the higher magnification in D).

To provide more rigorous evidence for the CW associations of TGB3, the TMV P30-GFP protein (Fig. 1E), which localizes to the PD (10, 12, 51), and TGB3 were coexpressed (Fig. 1F). The DsRed-TGB3 and P30-GFP proteins both formed paired punctate patterns of fluorescence along the CW, at or near the PD of adjacent cells, as indicated by the individual red and green spots and by the yellow overlapping foci (Fig. 1F). After plasmolysis, most of the DsRed-TGB3 and the P30-GFP remained at the CW, and numerous yellow foci were observed (along with individual red or green foci), suggesting a colocalization of the two proteins at the CW (Fig. 1G and H). These experiments are reminiscent of PSLV TGB3 localization in transgenic plants in which the protein was associated with peripheral vesicles that were thought to have originated from the cortical ER (50, 59). However, the affinities of the BSMV and PSLV TGB3 proteins for the CW appear to differ somewhat in the two experimental systems because a substantial proportion of BSMV TGB3 remained associated with the walls after plasmolysis, whereas the PSLV TGB3 protein expressed in transgenic plants retracted from the CW after plasmolysis (17).

Analysis of PSLV has revealed that hydrophilic regions at the N and C termini of the TGB3 protein, which are predicted to protrude into the ER lumen, are required for targeting to CW-associated peripheral vesicles (39, 49). Sequences near the C terminus of PSLV TGB3 have also been found to interfere with CW trafficking (47). To verify these results and to more clearly define signals that target BSMV TGB3 to the CW, we constructed three deletion mutants and fused these mutants to the C terminus of DsRed (Fig. 2). The N-terminal 15 amino acids (M-A-M-P-H-P-L-E-C-C-C-P-Q-C-L) were deleted to produce the DsRed-TGB3$_{16\text{-}155}$ mutant (Fig. 2A), the five C-terminal residues (L-S-S-K-R) were truncated to yield DsRed-TGB3$_{1\text{-}150}$ (Fig. 2D), and both the 15 N-terminal and the 5 C-terminal residues were excised to generate DsRed-TGB3$_{16\text{-}150}$ (Fig. 2G).

Two days after agroinfiltration of the N-terminal mutant DsRed-TGB3$_{16\text{-}155}$, epidermal cells viewed by DIC microscopy exhibited paired fluorescent foci similar to those of wt DsRed-TGB3 (Fig. 2A). Confocal microscopy of cells coexpressing DsRed-TGB3$_{16\text{-}155}$ and GFP-talin revealed that the majority of the DsRed remained associated with the calcofluor-stained CW after plasmolysis but that a small proportion of DsRed was present in the cytosolic fraction containing GFP-talin (Fig. 2B). The P30-GFP and DsRed-TGB3$_{16\text{-}155}$ fusion proteins both colocalized as paired foci at the CW after coinfiltrations (Fig. 2C, note the separate red, green, and overlaid channels).

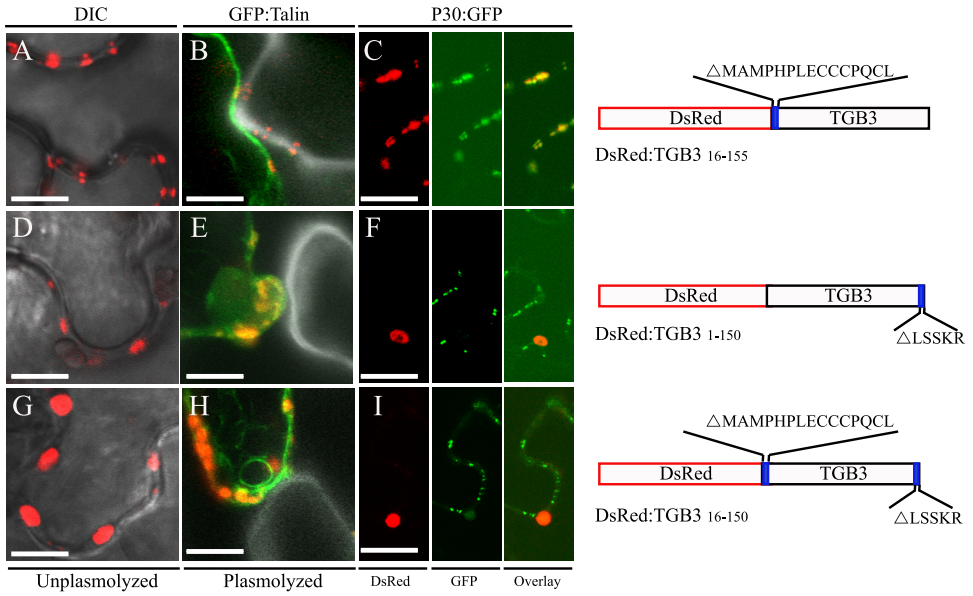

FIG. 2. Subcellular localization of TGB3 mutants. (A, D, and G) Appearance of cells in tissue infiltrated with *Agrobacterium* isolates harboring DsRed-TGB3 plasmid derivatives. Epifluorescent images are overlaid onto DIC images. (B, E, and H) Plasmolyzed cells in tissue expressing DsRed-TGB3 derivatives and GFP-talin. (C, F, and I) Plasmolyzed leaf cells coinfiltrated with DsRed-TGB3 derivatives and P30-GFP. (A to C) Paired CW foci formed after infiltration with the DsRed-TGB3$_{16\text{-}156}$ mutant, which lacks the first 15 N-terminal amino acids. (D to F) Cells expressing DsRed-TGB3$_{1\text{-}150}$, which has a truncation of the five C-terminal amino acids. (G to I) Tissue infiltrated with bacteria containing the DsRed-TGB3$_{16\text{-}150}$ TGB3 mutant with deletions of the first 15 N-terminal and the last 5 C-terminal amino acids. Note that the cartoons on the right illustrate the three TGB3 deletion mutants and highlight the deleted sequences. Bars, 20 μm.

In contrast, evidence from DIC microscopy revealed that the C-terminal deletion mutant DsRed-TGB3$_{1\text{-}150}$ often formed discrete globular structures around the periphery of the cell that did not appear to cross the CW (Fig. 2D). Additional experiments with coexpressed DsRed-TGB3$_{1\text{-}150}$ and GFP-talin showed that both proteins retracted into the cytoplasm after plasmolysis (Fig. 2E). In another experiment, the 5-amino-acid C-terminal deletion DsRed-TGB3$_{1\text{-}150}$ was coexpressed with the wall-associated TMV P30-GFP (52). After plasmolysis, DsRed-TGB3$_{1\text{-}150}$ detached from the CW and formed large globular structures in the cytoplasm, but P30-GFP remained at the CW (Fig. 2F). More pronounced globular structures were also noted when the DsRed-TGB3$_{16\text{-}150}$ mutant was expressed (Fig. 2G). This N- and C- terminal deletion mutant also failed to bind to the CW, as indicated by the fluorescence patterns after plasmolysis (Fig. 2H and I). These results thus suggest that the five C-terminal residues participate in interactions required for TGB3 attachment to the CW.

To provide a more definitive assessment of the requirements of the C-terminal region for CW localization, three additional TGB3 mutants were constructed to target the last two C-terminal residues postulated to protrude from the membrane (Fig. 3). The subcellular localization results with these mutants contrast those for the N-terminal mutant DsRed-TGB3$_{16\text{-}155}$, which remained associated with the CW (Fig. 3A). In these mutants, the deletion of a single R residue at position 155 (DsRed-TGB3$_{1\text{-}154}$) and a site-specific R-to-A substitution at position 155 (DsRed-TGB3$_{R155A}$) disrupted the ability of TGB3 to target the CW (Fig. 3B and C), and this same effect was noted for mutant DsRed-TGB3$_{1\text{-}153}$ when positions 154 and 155 were deleted (Fig. 3D) or when A-residue substitutions for the K and R residues (DsRed-TGB3$_{K154A,R155A}$) were incorporated (Fig. 3E). However, as will become apparent later, it is important that a small amount of red fluorescence remained at the CW along with the P30-GFP MP when the DsRed-TGB3$_{R155A}$ derivative was infiltrated (Fig. 3C). These results extend recently reported results for PSLV (47) and provide a strong argument indicating that the last two C-terminal amino acid residues have important effects on BSMV TGB3 localization at the CW.

TGB2 and TGB3 interactions are required for TGB2 targeting to the CW. In order to compare the localization patterns of TGB2, infiltration experiments were carried out with bacteria capable of expressing GFP-TGB2 from a single plasmid, with mixtures of bacteria capable of expressing GFP-TGB2 and GFP-TGB3 from separate plasmids, or with bacteria harboring the GFP-TGB2/3 plasmid in which TGB2 and TGB3 are translated from the same mRNA. When the GFP-TGB2 fusion protein was expressed alone, a distinctive network pattern of GFP-TGB2 fluorescence was detected in membranes distributed throughout the cell (Fig. 4A, top). These patterns appeared to be similar to those of the reticulated fluorescent membranes found in transgenic plants expressing the GFP-KDEL ER targeting sequence (Fig. 4A, bottom). Moreover, upon plasmolysis, the membranes collapsed to form large globular GFP-TGB2 structures with little evidence of a network structure (Fig. 4B). In contrast, when approximately equal amounts of GFP-TGB2 and GFP-TGB3 were expressed from bacteria harboring separate plasmids, a substantial proportion of the GFP-TGB2 fluorescence appeared as paired foci along the CW of infiltrated tissues, and there was little evidence of the cytosolic network pattern (Fig. 4C). However, these foci

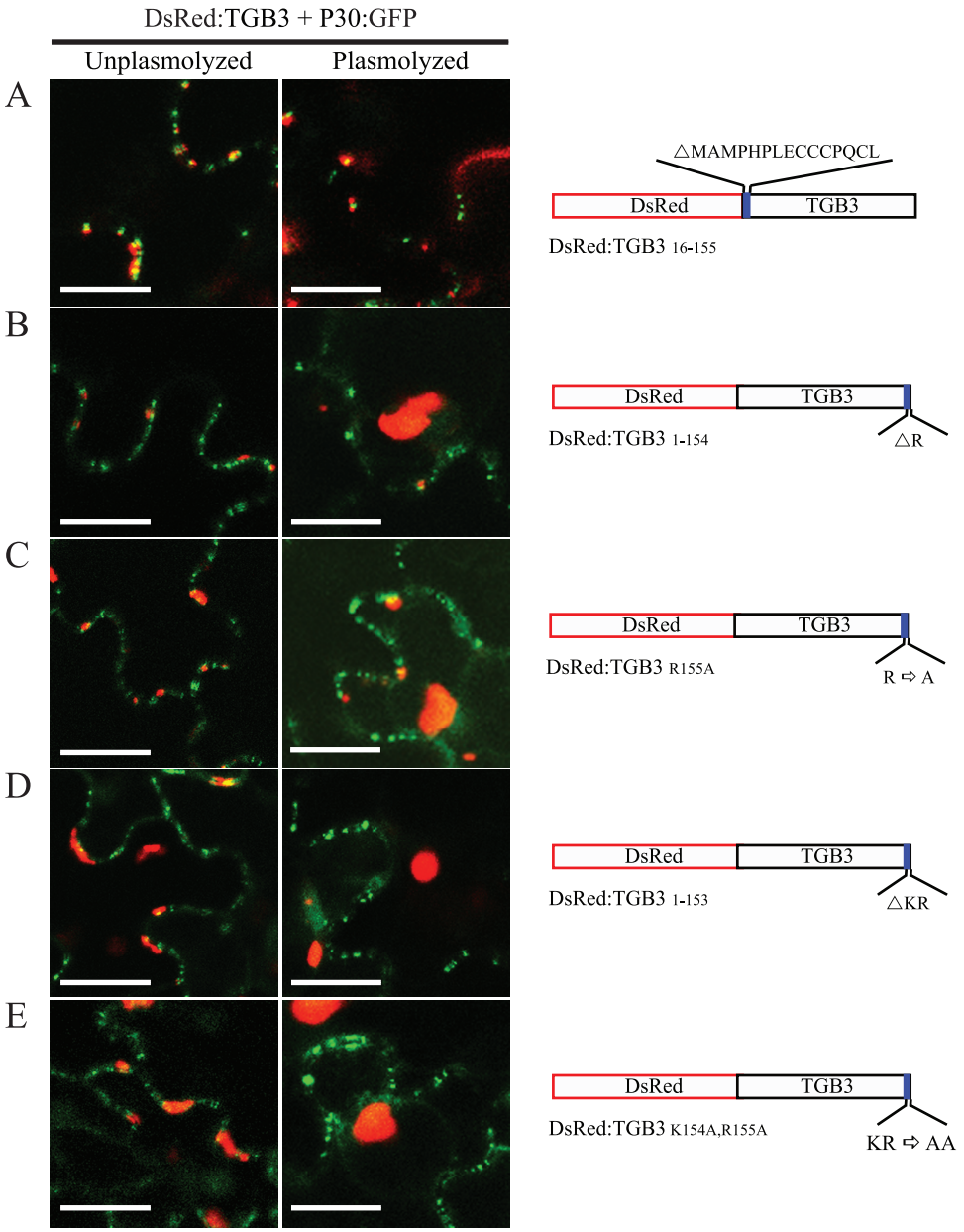

FIG. 3. Effects of DsRed-TGB3 deletions and amino acid substitutions on CW localization. Shown are appearances of leaf cells coexpressing TGB3 mutants and P30-GFP. (A) DsRed-TGB3$_{16\text{-}155}$; (B) DsRed-TGB3$_{1\text{-}154}$; (C) DsRed-TGB3$_{R155A}$; (D) DsRed-TGB3$_{1\text{-}153}$; (E) DsRed-TGB3$_{K154A,R155A}$. The DsRed-TGB3 mutants with altered sequences are illustrated in the cartoon to the right of the images. Plasmolyzed and unplasmolyzed cells are indicated above the respective panels. Bars, 20 μm.

were disrupted after plasmolysis, so it appeared that the CW associations were not stable (Fig. 4D). In contrast, when GFP-TGB2 and GFP-TGB3 were expressed from the GFP-TGB2/3 plasmid to permit translation from an mRNA corresponding to that occurring in viral infections (60), more stable associations of TGB2 occurred at the CW (Fig. 4E and F). In summary, the results provide strong evidence that TGB2 is associated with the membrane fraction when expressed alone but that when the ratios of TGB2 to TGB3 resemble those found for natural infections, a substantial proportion of TGB2 localizes at the CW.

We have recently constructed site-specific mutations that disrupt interactions between TGB2 and TGB3 and found that BSMV strains containing these mutations are unable to move from cell to cell (30). In order to determine the effects of these mutations on the subcellular localization of the TGB proteins, bacteria containing the mutant plasmid pGFP:TGB2$_{G40R,P41R}$/3 or pGFP:TGB2/3$_{P105R,I108R}$, whose substitutions each disrupt physical interactions between the two expressed proteins (30), were infiltrated into leaf tissue and evaluated by confocal microscopy 2 days later. In contrast to the CW targeting observed during the expression of GFP-TGB2/3 (Fig. 4E), GFP-TGB2$_{G40R,P41R}$/3, GFP-TGB2/3$_{P105R,I108R}$, and GFP-TGB2/3$_{1\text{-}150}$ expression resulted in a cytoplasmic localization

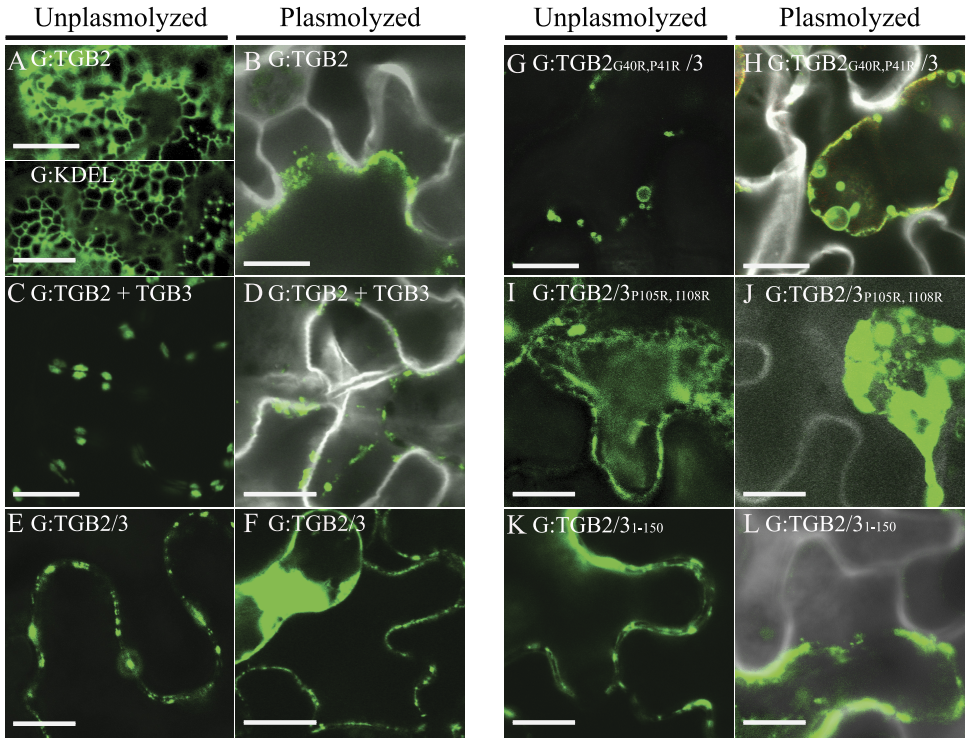

FIG. 4. Localization of the GFP-TGB2 fusion protein. Proteins were expressed in *N. benthamiana* leaves by agroinfiltration, and confocal images of epidermal cells were captured 2 to 3 days postinfiltration. (A) GFP-TGB2 (G:TGB2) network pattern and ER patterns in plants transformed with G-KDEL. (B) Plasmolyzed cells infiltrated with GFP-TGB2. (C) Paired foci formed in cells of leaf tissue infiltrated with separate plasmids for GFP-TGB2 and GFP-TGB3 designed to provide approximately equal amounts of GFP-TGB2 and GFP-TGB3. (D) CW foci after plasmolysis of leaves expressing GFP-TGB2 and GFP-TGB3. (E) Fluorescence patterns in leaves expressing the GFP-TGB2/3 plasmid to obtain ~10:1 ratios of TGB2 to TGB3. (F) Cells from plasmolyzed leaf tissue expressing GFP-TGB2/3. (G) Fluorescence of mutant GFP-$TGB2_{G40R,P41R}$/3. Note that the $TGB2_{G40R,P41R}$ mutation interferes with the heterologous binding of TGB2 to TGB3. (H) Plasmolyzed cells from leaves infiltrated with the GFP-$TGB2_{G40R,P41R}$/3 plasmid. (I) GFP-TGB2/$3_{P105R,I108R}$. Note that the $TGB3_{P105R,I108R}$ mutation disrupts TGB3 binding to TGB2. (J) Plasmolyzed cells in tissue expressing GFP-TGB2/$3_{P105R,I108R}$. (K) GFP-TGB2/3_{1-150}. Note that the $TGB3_{1-150}$ mutation prevents TGB3 binding to the CW. (L) Plasmolyzed cells expressing GFP-TGB2/3_{1-150}. Bars, 50 μm.

of fluorescence (Fig. 4G, I, and K). When the GFP-$TGB2_{G40R,P41R}$/3 mutant protein, which contains substitutions at TGB2 positions 40 and 41, was coexpressed with TGB3, the fluorescence of the mutant GFP-TGB2 protein was also distributed throughout the cytoplasm in nonplasmolyzed cells in association with large membrane vesicles (Fig. 4G). Fluorescence after plasmolysis confirmed that GFP-TGB2 was membrane associated and that the calcofluor-stained CWs did not contain fluorescent foci (Fig. 4H). In addition, the expression of GFP-TGB2/$TGB3_{P105R,I108R}$ led to the conclusion that the GFP-TGB2 wall association requires TGB3 binding (Fig. 4I and J). As anticipated from the results shown in Fig. 2, the GFP-TGB2/3_{1-150} mutant, in which the five C-terminal residues were deleted, also failed to localize to the CW (Fig. 4K and L). Together, these results indicate that mutations that disrupt the interactions between TGB2 and TGB3 or that interfere with CW targeting by TGB3 have dramatic effects on the localization of TGB2.

Optimal TGB1 CW localization requires interactions between TGB2 and TGB3. The available evidence indicates that the hordeivirus-like TGB1 proteins are cytoplasmically localized when expressed alone and require TGB2 and TGB3 for peripheral membrane/CW targeting in protoplasts and leaf cells (9, 15, 27, 39). Because of the difficulties in detecting interactions between TGB2 and TGB3, questions have been raised as to whether the TGB3-mediated targeting of TGB proteins involves direct physical interactions of the TGB proteins (39). However, we have shown that BSMV cell-to-cell movement is disrupted by amino acid substitutions that interfere with heterologous interactions between TGB2 and TGB3 (30). To obtain more detailed evidence concerning the mechanisms whereby TGB1 is localized to the PD and the roles of TGB3 in the cellular localization of TGB1, we carried out coinfiltrations with various combinations of TGB2 and TGB3 derivatives (Fig. 5 and 6).

Our previous results for protoplasts infected with BSMV mutants containing a deletion in TGB3 revealed that GFP-TGB1 is membrane localized (27). Similarly, GFP-TGB1 formed large bright fluorescent foci throughout the cytoplasm when expressed alone in *N. benthamiana* leaves (Fig. 5A), and punctate foci failed to form at the CW after plasmolysis (Fig. 5B and C). In addition, confocal microscopy of leaf cells coinfiltrated only with bacteria harboring GFP-TGB1 and GFP-TGB2 clearly revealed that GFP-TGB1 was membrane associated and retracted from the CW along with the DsRed-talin marker in plasmolyzed cells (Fig. 5E and F). When bacteria containing plasmids for the expression of approximately equal amounts of GFP-TGB1 and GFP-TGB3 were coinfiltrated

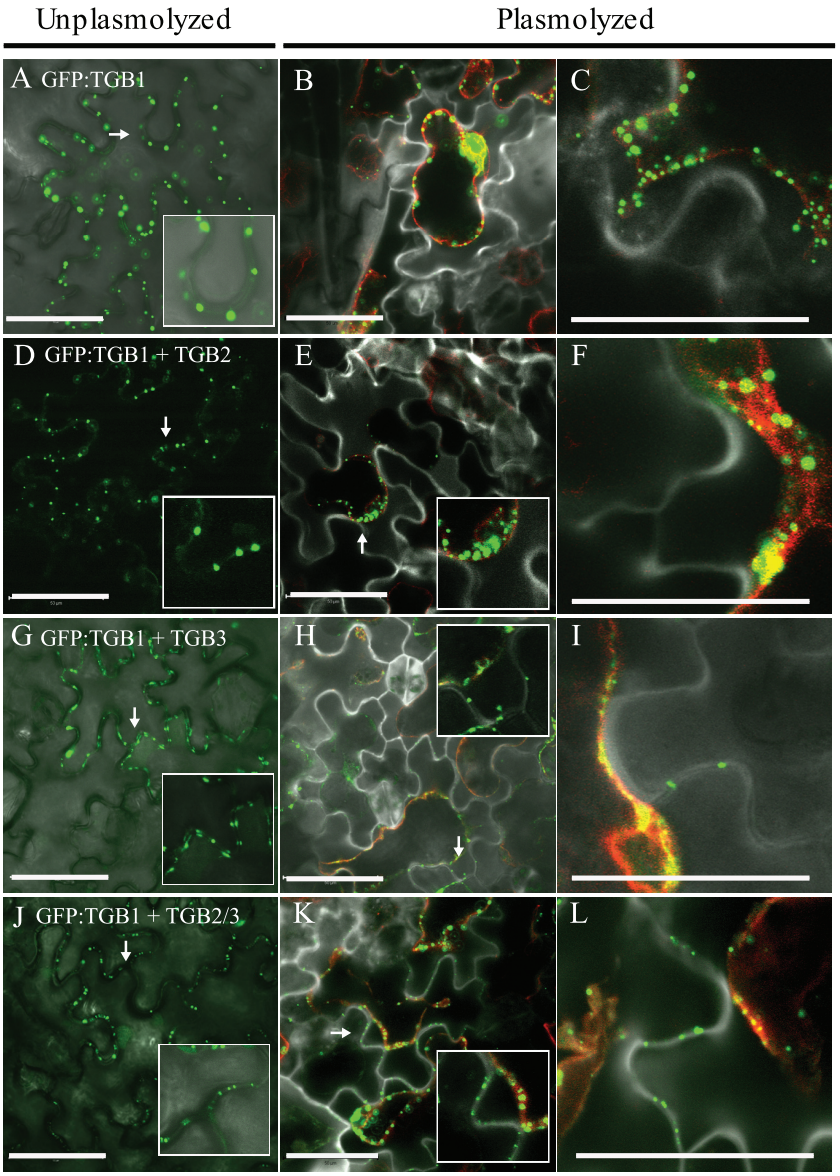

FIG. 5. TGB3-directed subcellular localization of TGB1. (A) GFP-TGB1-expressing cells showing fluorescent images overlaid onto DIC images. (B) GFP-TGB1 and DsRed-talin fluorescence in plasmolyzed cells. (C) Magnified plasmolyzed cell showing GFP-TGB1 and DsRed-talin fluorescence. (D) Fluorescence of GFP-TGB1 overlaid onto DIC images of cells coexpressing TGB2. (E) Plasmolyzed cells containing GFP-TGB1 and GFP-TGB2. (F) Magnified plasmolyzed cells coexpressing GFP-TGB1 and GFP-TGB2. (G) DIC images showing GFP-TGB1 fluorescence in cells coexpressing TGB3. (H) Plasmolyzed cell showing GFP-TGB1 fluorescence in the presence of TGB3. (I) Magnified image showing GFP-TGB1 in plasmolyzed cells containing TGB3. (J) DIC images showing localization of GFP-TGB1 in the presence of TGB2/3. (K) Plasmolyzed cells expressing GFP-TGB1 and GFP-TGB2/3. (L) Magnified image showing GFP-TGB1 and GFP-TGB2/3 in plasmolyzed cells. Bars, 50 μm.

(Fig. 5G to I), a considerable amount of the fluorescence also retracted into the cytosol upon plasmolysis, but a small amount of fluorescence consistently remained associated with the CW (Fig. 5H and I). In marked contrast, leaves coinfiltrated with bacteria containing the GFP-TGB1 and GFP-TGB2/3 plasmids (Fig. 5J to L), to provide ratios of TGB2 to TGB3 similar to those for viral infections (60), consistently resulted in higher levels of wall-associated foci in the plasmolyzed cells, although a substantial proportion of the GFP remained in the cytoplasm (Fig. 5K and L). These results suggest that TGB2 has little direct influence on TGB1 localization and that TGB3 mediates the CW targeting of TGB1. However, the results also indicate that TGB3 alone is not sufficient for the optimal targeting of TGB1 to the CW, so we hypothesized that the ratios of TGB2 and TGB3 are important for optimal TGB1 CW localization.

Ratios of expression levels of TGB2 to expression levels of TGB3 affect the subcellular localization of TGB1 and TGB2. During BSMV infections, the TGB2 and TGB3 genes are expressed from overlapping reading frames on low-abundance sgRNAβ2 (60). Ribosomes initiating at the first AUG codon of sgRNAβ2 result in TGB2 translation, and TGB3 protein translation is initiated at a second alternative frame via leaky ribosomal scanning. This mechanism yields approximately 10-fold-larger amounts of TGB2 than TGB3 during the translation of

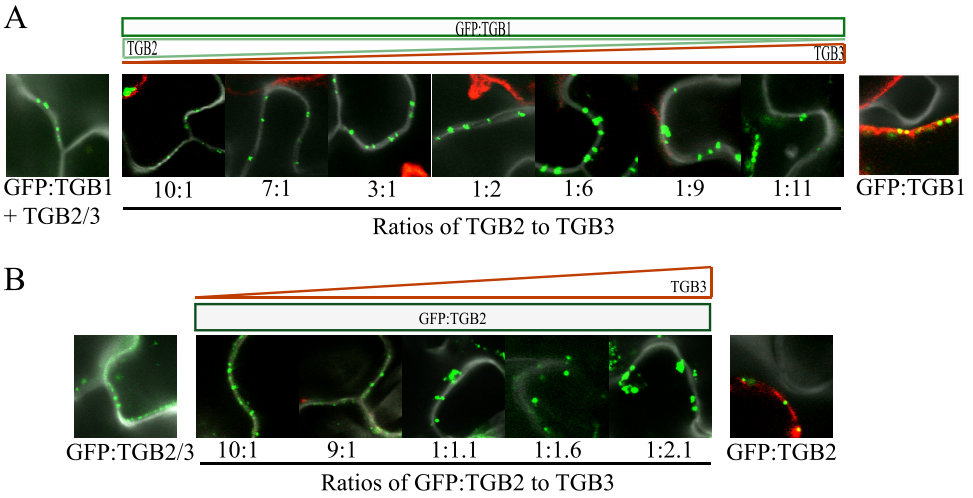

FIG. 6. Subcellular localization of GFP-TGB1 and GFP-TGB2 during expression of various ratios of TGB2 toTGB3. (A) Confocal laser scanning microscopy of plasmolyzed leaf epidermal cells infiltrated with mixtures containing equal amounts of *Agrobacterium* strains harboring the GFP-TGB1 plasmid and various ratios of strains containing the TGB2 and TGB3 plasmids. DsRed-talin serves as a membrane marker. (Far left) Localization pattern of GFP-TGB1 in the presence of TGB2/3. (Far right) Localization of GFP-TGB1 alone. Ratios of mRNA expression levels of TGB2 to those of TGB3 were estimated by real-time PCR as shown in Table 2. The green rectangle indicates constant levels of GFP-TGB1 mRNA, the green triangle indicates estimated decreases in TGB2 mRNA levels, and the red triangle shows increases in TGB3 mRNA levels. The calculated TGB2-to-TGB3 ratios are indicated below each image. (B) Cells expressing constant levels of GFP-TGB2 with increasing amounts of TGB3 elicited by infiltration mixtures varying between 10:1 and 1:1 as shown in Table 3. The green rectangle indicates constant levels of GFP-TGB2 mRNA, and the red triangle represents increasing levels of TGB3 mRNA. The calculated TGB2-to-TGB3 ratios are designated below each image. The localization of GFP-TGB2 expressed from the GFP-TGB2/3 construct is shown at the far left, and that of GFP-TGB2 is shown at the far right. Note that confocal laser scanning microscopy images of plasmolyzed epidermal cells were captured at 2 days postinfiltration. CWs were stained with calcofluor blue, and DsRed-talin was used to visualize the cytoplasm and membrane fractions. The relative ratios of expression levels of TGB2 and TGB3 mRNAs were estimated by real-time PCR using the $2^{-\Delta CT}$ calculation method described in Materials and Methods (Table 3). Each panel shows a 20-μm^2 region.

BSMV sgRNAβ2 (60). In our previous study, we engineered a quadripartite virus designed to express TGB1, TGB2, and TGB3 in *cis* or in *trans*, and the results demonstrated that cell-to-cell virus movement is abrogated when TGB2 and TGB3 are expressed in *trans* from different sgRNAs (30). Moreover, we were able to demonstrate that the ratios of expression of TGB2 and TGB3 in *cis* have marked effects on the extent of the cell-to-cell movement of the virus (30).

To evaluate our hypothesis that varied ratios of TGB2 and TGB3 expression levels affect the subcellular localization of the TGB1 and TGB2 proteins, separate plasmids were designed for uncoupled expression to produce approximately equal amounts of TGB2 and TGB3, or a single plasmid (pGD2/3) was designed to provide ~10:1 ratios of TGB2 to TGB3 from a single mRNA analogous to sgRNAβ2 (60). Variable amounts of *Agrobacterium* suspensions harboring these plasmids were coinfiltrated into *N. benthamiana* leaves to mediate different levels of protein expression. This method was described previously, and we were able to demonstrate that the ratios of the TGB proteins can be manipulated by varying the concentrations of infiltrated bacteria expressing each of the proteins (30). Because we have been unable to raise highly specific antibodies against TGB3 (14), the abundances of the TGB1, TGB2, and TGB3 transcripts relative to *N. benthamiana ACTIN* (GenBank accession no. AY179605) transcripts were estimated at 2 days postinfiltration by real-time quantitative PCR using the $2^{-\Delta\Delta CT}$ method (34). Each infiltration experiment with bacterial concentrations designed for the expression of different ratios of TGB2 to TGB3 was repeated using four or five individual plants. Confocal laser scanning microscopy of the leaf samples was also carried out at 2 days postinfiltration to evaluate the subcellular localization of the fluorescent fusion proteins, and these results were compared with the PCR results showing the relative levels of expression of each of the RNAs (Table 2).

In the experiments shown in Fig. 6A, the *Agrobacterium* strain containing the TGB1 expression plasmid was kept constant in all treatments, and the levels of mRNA expression of TGB2 and TGB3 varied proportionately with the ratios used for other coinfiltration mixtures (Table 2). Microscopy experiments revealed that the CW localization of GFP-TGB1 varied depending on the ratios of the level of expression of TGB2 to that of TGB3 (Fig. 6A). When the TGB2/3 plasmid for the expression of ~10:1 TGB2-to-TGB3 ratios was coinfiltrated with the GFP-TGB1 plasmid, sharp punctate fluorescent spots appeared to localize within the PD of the plasmolyzed cells (Fig. 6A, far left). In addition, when TGB2 and TGB3 were expressed from different plasmids during mixed infiltrations in which the bacterial ratios were adjusted to yield TGB2-to-TGB3 ratios of ~10:1, the patterns of GFP-TGB1 fluorescence in plasmolyzed cells were very similar to those resulting during the coexpression of TGB2/3 and GFP-TGB1 (Fig. 6A, left). However, as the mixtures of bacteria were altered to produce decreasing TGB2-to-TGB3 mRNA ratios, GFP-TGB1 formed progressively larger globular fluorescent spots along the plasmolyzed CW, and at the lowest TGB2-to-TGB3 ratios, when a ~10-fold excess of TGB3 mRNA was estimated, the spots detached from the CW and appeared in the cytoplasm along

TABLE 3. Quantitative PCR transcript levels in *N. benthamiana* leaf tissue infiltrated with various ratios of TGB2 to TGB3 in *Agrobacterium* cultures

Agrobacterium culture ratio (TGB2 to TGB3)[a]	Amt of inoculum (μl)			No. of plants	Mean relative TGB2/TGB3 quantitative PCR transcript level ± SD[b]
	pGDG:TGB2	pGD:TGB3	pGD		
10:1	400	40	560	4	8.7 ± 1.3
1:1	220	220	560	4	0.9 ± 0.4

[a] All cultures have an optical density at 600 nm of 0.6.
[b] $2^{-\Delta\Delta CT} = 2^{-[\Delta CT(GFP\text{-}TGB2\text{-}actin) - \Delta CT(TGB3\text{-}actin)]}$.

with the DsRed-talin marker protein (Fig. 6A, right). These patterns were similar to those observed when GFP-TGB1 and the DsRed-talin marker were coexpressed in the absence of TGB2 and TGB3 (Fig. 6A, far right, and Fig. 5A to C, respectively).

In a second set of experiments, different ratios of GFP-TGB2 to GFP-TGB3 were tested to assess the influence of their relative abundances on TGB2 localization. Bacterial mixtures designed for the expression of 10:1 to <1:2 ratios of GFP-TGB2 to GFP-TGB3 were infiltrated, and the TGB2 and TGB3 mRNA levels again varied proportionately with the ratios of bacteria used in the infiltration mixtures (Table 3). At mRNA ratios near 10:1, the fluorescence of GFP-TGB2 appeared as sharp foci that spanned the plasmolyzed CW (Fig. 6B, left). However, at mRNA ratios of GFP-TGB2 to GFP-TGB3 of approximately 1:1 to 1:2, GFP-TGB2 formed larger spots that detached from the wall during plasmolysis (Fig. 6B, right). Thus, GFP-TGB2 foci at the higher ratios of GFP-TGB2 to GFP-TGB3 more closely resembled the patterns formed by TGB2/3 (Fig. 6, far left), whereas those that formed at the lower mRNA ratios of GFP-TGB2 to GFP-TGB3 retracted from the CW although to a lesser extent than when GFP-TGB2 was expressed alone (Fig. 6B, far right). In toto, these experiments indicate that the relative ratios of TGB2 and TGB3 expression are critical for the ability of TGB3 to direct TGB1 and TGB2 to the PD efficiently and suggest that TGB2-to-TGB3 ratios similar to those expressed from wt BSMV are important for the appropriate subcellular targeting of both TGB1 and TGB2.

Interactions of TGB3 with TGB2and TGB3 C-terminal amino acids are essential for optimal CW targeting of TGB1. To provide additional evidence to evaluate the roles of TGB2 and TGB3 in TGB1 targeting, a second series of coinfiltration experiments was carried out with bacteria harboring the membrane marker DsRed-talin, the GFP-TGB1 plasmid, and various TGB2/3 derivatives (Fig. 7). As anticipated from the experiments described above, the coexpression of GFP-TGB1 along with the TGB2/3 plasmid for the expression of TGB2 and TGB3 from the same mRNA resulted in a large number of TGB1 foci associated with the calcofluor-stained CWs of plasmolyzed cells, whereas DsRed-talin retracted with the cytoplasm (Fig. 7A). However, when GFP-TGB1 was coexpressed with $TGB2_{G40R,P41R}/3$, which interferes with the ability of TGB2 to interact with TGB3 (30), GFP-TGB1 was largely cytoplasmic (Fig. 7B). Moreover, in the presence of the TGB2/$3_{P105R,I108R}$ mutant derivative, which also affects heterologous associations of TGB2 and TGB3 (30), only a small proportion of GFP-TGB1 formed CW foci, and almost all of the fluorescence retracted into the cytosol with DsRed-talin when cells were plasmolyzed (Fig. 7C). In addition, when the GFP-TGB1- and DsRed-talin-containing bacterial strains were coinfiltrated along with the TGB2/$3_{1\text{-}150}$ mutant, GFP-TGB1 was no longer targeted to the CW, and both GFP-TGB1 and DsRed-talin colocalized with the plasmolyzed cytosolic fraction (Fig. 7D). These results were anticipated from the results in Fig. 2 and 3, which show that several mutations affecting the C-terminal TGB3 residues reduce TGB3 CW associations. In summary, results for the TGB3 mutant provide confirmatory evidence that the C-terminal region of TGB3 is critical for CW associations and that TGB2 and TGB3 interactions have functional roles in TGB1 CW associations.

TGB1 helicase motif mutants have variable CW targeting effects. Site-specific mutations introduced into six conserved regions of the C-terminal TGB1 helicase domain were previously shown to interfere with BSMV infection of barley (27). In addition, several helicase mutations altered the subcellular distribution of GFP-TGB1 in protoplasts infected with BSMV. The fluorescent patterns in infected protoplasts ranged from punctate foci appearing at the plasma membrane for wt GFP-TGB1 to a disperse cytoplasmic pattern with TGB1 mutants containing site-specific mutations in the helicase motifs (27). In addition, we have used affinity chromatography (30) to demonstrate that TGB1-homologous interactions are disrupted by mutations within helicase domain I mutant M2 (K259A) and domain II mutant M3 (D313N and E314N) but not by domain IV mutant M5 (R368A) or domain VI mutant M7 (R464A). These results thus raised questions about the abilities of TGB1 with mutations in these domains to be targeted to the CW.

In agroinfiltration control experiments lacking TGB2/3, the

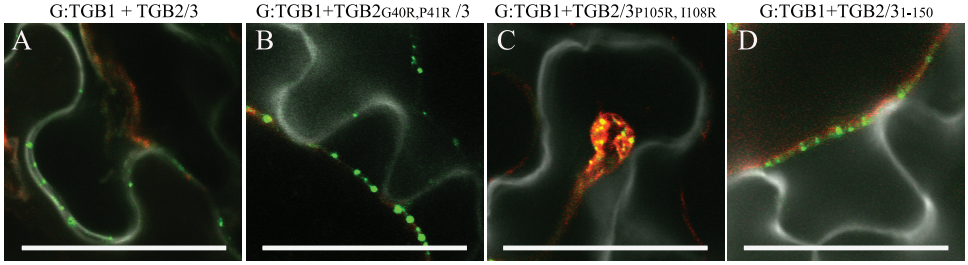

FIG. 7. TGB1 localization in cells coexpressing TGB2 and TGB3 mutant proteins. (A) GFP-TGB1 (G:TGB1) fluorescence during coexpression of TGB2/3 to elicit ~10:1 ratios of TGB2 to TGB3. (B) $TGB2_{G40R,P41R}/3$. (C) TGB2/$3_{P105R,I108R}$. (D) TGB2/$3_{1\text{-}150}$. All panels show plasmolyzed cells, and DsRed-talin serves as a cytoplasmic marker. Bars, 50 μm.

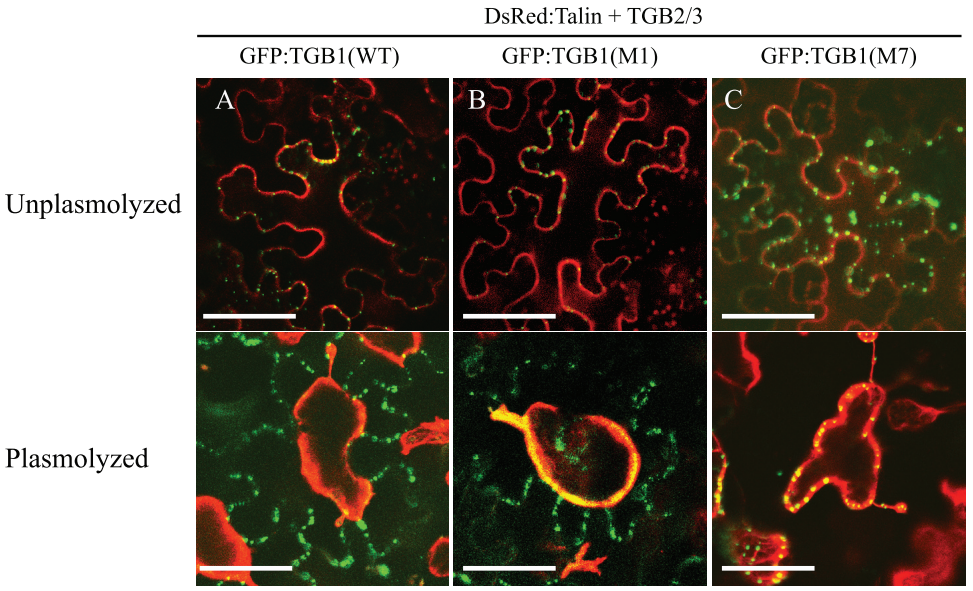

FIG. 8. Variable effects of helicase motif mutants on TGB1 targeting. (A) CW-associated fluorescence of wt GFP-TGB1 in unplasmolyzed and plasmolyzed cells coexpressing TGB2/3 and DsRed-talin. (B) GFP-TGB1 M1 mutant localization in cells coexpressing TGB2/3 and DsRed-talin. (C) GFP-TGB1 M7 mutant associations during coexpression with TGB2/3 and DsRed-talin. Note the large spots associated with the plasmolyzed protoplast and the absence of fluorescence at the CW after plasmolysis. Bars, 50 μm.

localization patterns of the GFP-TGB1 M1 (K259R), M2, M3, M4 (G339A, D340N, and Q343E), M5, and M7 mutants were evaluated directly in companion experiments. The GFP-TGB1 M5 and M7 mutants were cytoplasmic both before and after plasmolysis when expressed in the absence of TGB2/3. Moreover, in all cases, the helicase mutants were indistinguishable from those of wt GFP-TGB1 after plasmolysis in that almost all of the fluorescence retracted into the cytoplasm along with the cytoplasmic marker DsRed-talin (data not shown). In agreement with results described above (Fig. 6A and 7), when bacteria harboring GFP-TGB1 were coinfiltrated with those specifying pGD:TGB2/3, most of the wt GFP-TGB1 fluorescence remained at the CW after plasmolysis and was distinct from that of DsRed-talin (Fig. 8A). However, when the GFP-TGB1 M7 mutant was coexpressed with TGB2/3, green fluorescence was present in the cytoplasm along with DsRed-talin after plasmolysis (Fig. 8C), and similar results were obtained with the M3, M4, and M5 mutants (data not shown). Surprisingly, a different pattern emerged when the TGB1 M1 mutant was coexpressed with TGB2/3. In this case, much of the GFP-TGB1 fluorescence remained at the CW after plasmolysis (Fig. 8B). However, as illustrated by the yellow color in the membrane fraction, a somewhat greater proportion of the fluorescence from the M1 mutant retracted with DsRed-talin after plasmolysis than was observed with wt GFP-TGB1. A similar pattern was also observed with the GFP-TGB1 M2 mutant, which affects the same amino acid residue as the M1 mutant (data not shown). Therefore, because the M1 mutant interferes with TGB1 binding (32), our interpretation is that homologous interactions are not absolutely essential for CW targeting and that the M3, M4, M5, and M7 mutants are involved in other cellular interactions required for CW targeting.

Dysfunctional TGB2 and TGB3 mutants affect movement and TGB1 localization in BSMV-infected plants. We have previously shown that inoculum containing RNAα, RNAβ, and RNAγ-γb-GFP provides a useful reporter that can be used to assess BSMV movement effects in *N. benthamiana* (27, 30). Using this reporter virus, we determined that several RNAβ derivatives containing single TGB1 helicase motif mutants were unable to function in cell-to-cell movement (27). More recently, we have shown that fluorescent foci were confined to single cells of leaves inoculated with RNAβ reporter derivatives containing site-specific mutations in TGB2 and TGB3 that interfere with the ability to form heterologous binding interactions (30). In order to determine the effects of additional TGB3 mutants used in the experiments described above, we carried out a series of infectivity experiments with the reporter virus (Fig. 9). The results revealed that the wt RNAβ reporter virus developed fluorescent foci composed of several hundred cells by 7 dpi and that the foci continued to spread radially over the next 3 days (Fig. 9A). In contrast, leaves inoculated with reporter virus containing the RNAβ $TGB3_{P105R,I108R}$ mutation, which destroys interactions with TGB2, developed numerous single-cell fluorescent foci that failed to move beyond the initially infected cells (Fig. 9B and data not shown). Similar results were obtained for leaves rubbed with inocula containing the $TGB3_{1-153}$ deletion mutant (Fig. 9C) and the $TGB3_{K154A,R155A}$ substitution mutant (Fig. 9D), each of which targets the two C-terminal amino acid residues of the protein. An additional mutant, $TGB3_{R155A}$, had only limited cell-to-cell movement, encompassing an estimated 50 cells at 7 dpi, and subsequent evaluations indicated that the fluorescent foci had only marginal increases in diameter by 10 dpi (Fig. 9E). The effects of the $TGB3_{R155A}$ mutant were of particular interest because it reduced, but failed to completely eliminate, CW targeting of DsRed-TGB3 (Fig. 3C). Hence, it appears that the substitution of the C-terminal 155R residue

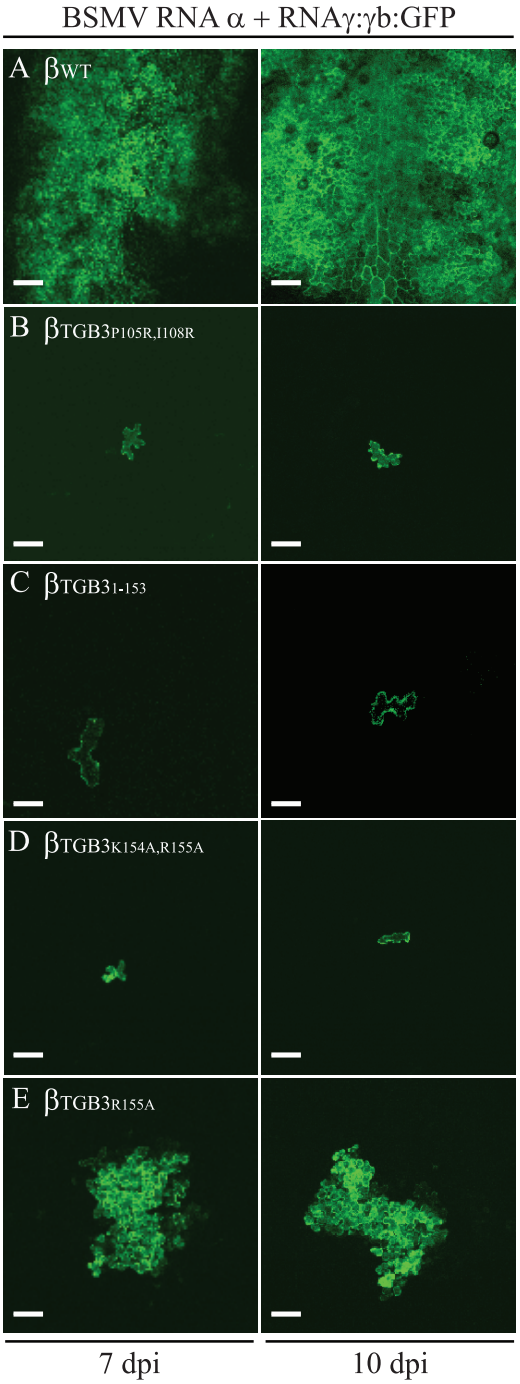

FIG. 9. Cell-to-cell movement of BSMV derivatives containing TGB3 mutations. *N. benthamiana* leaves were inoculated with infectious transcripts of BSMV ND18 wt RNAα and RNAγ-γb, with GFP to serve as a visual marker to assess localized movement and various RNAβ TGB2/3 mutants. (A) RNAβ wt. (B) $TGB3_{P105R,I108R}$, which interferes with heterologous interactions of TGB2 and TGB3. (C) $TGB3_{1-153}$, which has a truncation of the last two TGB3 C-terminal residues. (D) $TGB3_{K154A,R155A}$,with A-residue substitutions for the C-terminal K and R residues. (E) $TGB2/3_{R155A}$, with an A substitution for the C-terminal R residue. Note that the panel designations refer to RNAβ TGB2/3 derivatives that are expressed in the wt virus context, which results in a ~10:1 ratio of TGB2 to TGB3. Inoculated leaf samples were maintained in a growth chamber as described in Materials and Methods and photographed at 7 or 10 dpi. Bars, 50 μm.

does not totally compromise either CW targeting or the cell-to-cell movement of BSMV.

In order to monitor the localization of TGB1 during BSMV infections and to determine the validity of our ectopic expression results with the agroinfiltrated TGB1 proteins, we incorporated TGB2 and TGB3 mutations into RNAβ-GFP-TGB1 (27). This reporter virus was previously used to demonstrate that GFP-TGB1 is localized to the PD during infection of *N. benthamiana* leaves and that the fusion protein forms fluorescent foci at the plasma membrane of infected protoplasts (27). In addition, we used the GFP-TGB1 reporter virus to evaluate mutations incorporated into the helicase motif of GFP-TGB1 or deletions within TGB2 or TGB3 that result in a cytoplasmic localization of GFP-TGB1 fluorescence in infected protoplasts (27).

As previously demonstrated (27), *N. benthamiana* leaves rubbed with inocula containing wt RNAβ-GFP-TGB1 and examined at 9 dpi developed large numbers of CW-associated foci at the periphery of expanding infection sites in unplasmolyzed leaf tissue (Fig. 10A). Similar wall-associated foci and some cytosolic fluorescence associated with DsRed-talin were also present in plasmolyzed leaf tissue. In contrast, fluorescent foci were detected exclusively in the cytoplasm of leaf cells infected with mixtures containing RNAβ-GFP-TGB1 and TGB2 or TGB3 mutations affecting TGB2 and TGB3 interactions or mutants that affected TGB3 CW localization (Fig. 10B to E). These included the site-specific $TGB2_{G40R,P41R}$ (Fig. 10B) and $TGB3_{P105,I108R}$ (Fig. 10C) interaction mutations, the $TGB3_{1-153}$ (Fig. 10D) deletion mutation, and the $TGB3_{K154A,R155A}$ substitution mutation (Fig. 10E). In agreement with the results shown in Fig. 9E, leaves inoculated with mixtures containing the $TGB3_{R155A}$ mutant formed limited foci with greatly restricted cell-to-cell movement compared to the wt reporter virus (data not shown). Cells infected with the $TGB3_{R155A}$ mutant also contained some fluorescent GFP-TGB1 foci at the CW (Fig. 10F). In agreement with the TGB3 ectopic experiments shown in Fig. 3C, the proportion of wall-associated fluorescence in leaf cells infected with the wt GFP-TGB1-RNAβ reporter appeared to be higher than that in cells infected with the $TGB3_{R155A}$ substitution mutant (compare Fig. 10A and F), suggesting that the reduced rates of cell-to-cell movement result from a reduced ability of the $TGB3_{R155A}$ mutant to facilitate TGB1 wall associations. Overall, the infectivity results verify that the GFP-TGB1 localization patterns of the reporter virus derivatives correspond well with those of the mutant derivatives introduced into cells by agroinfiltration.

DISCUSSION

We have used *Agrobacterium* expression of GFP and DsRed fusions to BSMV TGB proteins in order to evaluate the cytoplasmic localization of different combinations of native and mutant protein derivatives. The use of agroinfiltration has obvious advantages over the use of transgenic plants in the time required to complete experiments, in the variety of derivatives that can be evaluated, and in the diversity and costs of individual experiments while reducing unanticipated effects of gene silencing that may affect protein expression (16). The advantages over particle bombardment or protoplasts include relatively limited cell stress or CW injury, the ability to intro-

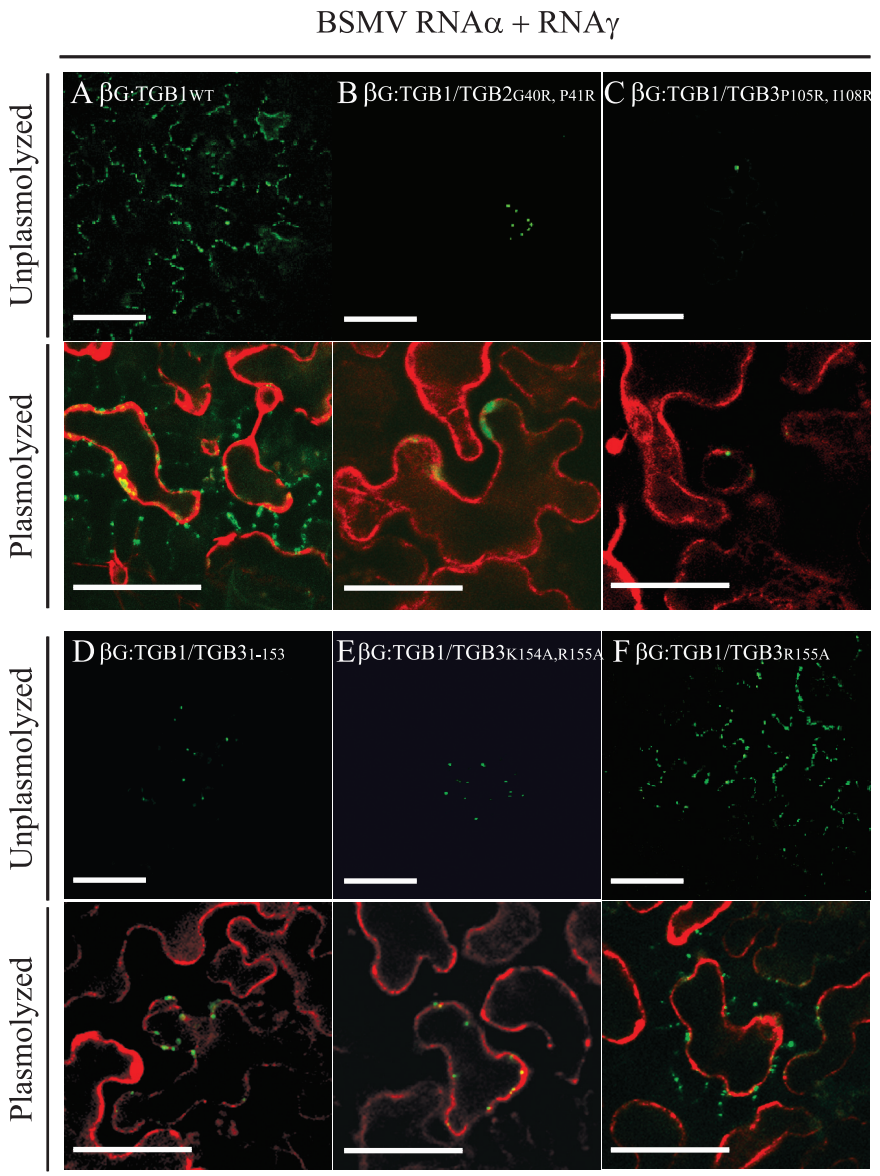

FIG. 10. Effects of TGB2 and TGB3 mutations on CW targeting by GFP-TGB1. (A) wt RNAβ-GFP-TGB1. (B) RNAβ-GFP-TGB1 containing the $TGB2_{G40R,P41R}$ mutation to disrupt TGB2 interactions with TGB3. (C) RNAβ-GFP-TGB1 with the $TGB3_{P105,I108R}$ mutation, which disrupts TGB3 interactions with TGB2. (D) RNAβ-GFP-TGB1 harboring the $TGB/3_{1-153}$ deletion mutant. (E) RNAβ-GFP-TGB1 containing the $TGB3_{K154A,R155A}$ substitution mutant. (F) RNAβ-GFP-TGB1 with $TGB3_{R155A}$. Note that *N. benthamiana* leaves were inoculated with infectious BSMV ND18 RNAα and RNAγ transcripts plus the RNAβ-GFP-TGB1 derivatives specified. Leaves to be plasmolyzed were infiltrated with *Agrobacterium* cells harboring DsRed-talin at 7 dpi, and the fluorescence of plasmolyzed or unplasmolyzed samples was observed at 9 dpi. Bars, 50 μm.

duce several bacteria harboring different expression derivatives from diverse sources into a large number of cells, and assurance that more than 95% of the cells in an infiltrated area will coexpress several proteins from multiple infiltrated bacteria and that expression patterns of the transiently expressed proteins reflect those of other cellular systems such as yeast and plant species. However, a relevant question concerning all ectopic experiments, including those derived from agroinfiltration, is the extent to which the results can be interpreted in the context of viral infections. To address this issue, we have investigated the effects of TGB2 and TGB3 mutations on TGB1 localization during infection with reporter viruses that were constructed in previous studies (27, 28). As discussed below, the infectivity results show very good agreement with the agroinfiltration findings and increase our confidence that the data which we have obtained can be interpreted in a biological context.

Our experiments clearly show that the BSMV TGB3 fusion protein, when expressed alone, forms punctate foci at calcofluor-stained walls that are resistant to plasmolysis. Many of the foci appear on opposite sides of the CW, suggesting a PD association, and they colocalize with TMV P30, which was used as a CW and PD marker (10, 12, 52). In mutagenesis experiments to determine the localization requirements of the 155-

amino-acid BSMV TGB3 protein, we found that the deletion of the two C-terminal K and R residues that are thought to protrude into the lumen of the ER were sufficient to eliminate CW localization. Moreover, the substitution of A residues for the K and R residues ($TGB3_{K154A,R155A}$) resulted in a dramatic retraction of TGB3 from the wall into the membrane fraction during plasmolysis. In addition, the substitution of a single A for the C-terminal R residue ($TGB3_{R155A}$) had an intermediate effect that reduced, but did not eliminate, foci remaining at the CW. The cellular effects of these two mutations are also correlated with the infectivity experiments because the RNAγ-GFP reporter virus containing the $TGB3_{K154A,R155A}$ mutation was unable to move from the initially infected cells, whereas limited cell-to-cell movement of the virus containing the $TGB3_{R155A}$ mutation was observed. These results provide persuasive evidence that the two C-terminal residues of the BSMV TGB3 protein are critical for CW targeting during the autonomous expression of the protein and that infectivity results with BSMV reporter derivatives demonstrate a biological context for the mutations by showing that the TGB3 mutants result in compromised movement phenotypes.

Our conclusion that TGB3 participates in CW targeting is also consistent with data from previous studies using varied approaches that have implicated the hordeivirus-like TGB3 proteins in PD-targeting activities (9, 17, 18, 49, 58, 59), and our data complement and extend recent findings in which a series of insertion, deletion, and site-specific mutations were used to provide an assessment of the CW targeting requirements of the PSLV TGB3 protein (47). These results also highlight functional differences between the hordeivirus-like TGB3 proteins with two membrane-spanning domains and those known to occur with the potexvirus-like single-membrane-spanning-domain TGB3 proteins. In the latter case, several investigations have shown that the potexvirus-like TGB3 proteins lack CW targeting activity and that they localize to the ER in leaf cells of *N. benthamiana*, *Nicotiana tabacum*, and additional hosts (26, 46). More recent findings revealed an association of the Potato *virus X* (PVX) TGB3 protein within large granular masses surrounding the nuclei of infected protoplasts that are enriched in ER membranes that appear to be distinct from the membrane anomalies observed when the TGB2 protein is expressed alone (45). These results in toto illustrate vast differences in the functional activities of the hordeivirus-like and potexvirus-like TGB3 proteins and reinforce hypotheses that quite distinct mechanisms have evolved to support the movement of viruses encoding the two classes of MPs (39, 54).

The functional roles of TGB2 in the subcellular interactions required for the cell-to-cell movement of associated nucleocapsid complexes are unclear. However, the two classes of TGB2 MPs have common features in that both classes have two membrane-spanning domains and a conserved region in the central domain (39). Both classes of TGB2 proteins can mediate the cell-to-cell movement of GFP or GFP-tagged fusion proteins (18, 51, 53), suggesting that TGB2 may function to increase PD size exclusion limits. Previous results with PVX TGB2 fluorescent fusion proteins expressed from a viral replicon have shown that the autonomously expressed proteins localize to reticulated regions thought to be derived from the ER (21, 26, 38). In recent studies in which the PVX TGB2 and TGB3 proteins were expressed ectopically in leaf cells, both proteins appeared in overlapping ER-derived granular vesicles (45). Our results with BSMV also revealed that autonomously expressed TGB2 localizes to network regions of the ER. In addition, a recent study also showed that BSMV TGB2, when expressed alone in bombarded cells, appears in abnormal membranes, and small amounts are localized in pleomorphic vesicles in the cytoplasm (53). Of particular significance, a small fraction of GFP-TGB2 was associated with invaginations that formed along the surface of chloroplasts when the GFP-TGB2 expression plasmid was cobombarded into cells along with RNAs α and γ (53). These invaginations appear to have been elicited in response to viral infection, and they may correspond to possible sites of BSMV replication in chloroplasts and proplastids of BSMV-infected wheat leaf and root tissue (31, 32).

Our results also confirm previous studies with hordeivirus-like TGB proteins showing that TGB2 exhibits a profound shift to the CW when the TGB2 and TGB3 proteins are coexpressed (17, 50, 58, 59). These results, along with those showing a similar GFP-TGB1 CW shift, demonstrate that ratios of expression levels of TGB2 to expression levels of TGB3 similar to those occurring during virus infections are essential for optimal CW targeting. This was particularly evident during our comparisons in which TGB2 and TGB3 were coexpressed from separate bacteria to produce approximately equal amounts of the two proteins versus those of bacteria expressing the TGB2/3 mRNA derivative, which leads to ~10-fold-greater amounts of TGB2 than TGB3 (60). The ectopic alteration of TGB2-to-TGB3 ratios also has pronounced effects on virus movement in plant cells, as we have shown in previous experiments when elevated amounts of TGB3 were generated from a viral replicon in inoculated tissue (30). Hence, our cytological results with altered ratios of TGB2 and TGB3 confirm previous findings that BSMV TGB3 overexpression interferes with TGB1 and TGB2 targeting to the CW and blocks cell-to-cell movement.

Because of difficulties in detecting interactions between TGB2 and TGB3, questions have been raised as to whether the TGB3-mediated targeting of TGB proteins involves a direct physical binding of the two proteins (39). However, this view does not explain the heterologous binding previously reported for the hordeivirus-like *Potato mop-top virus* (PMTV) TGB2 and TGB3 proteins (9). We have recently provided evidence to support the results of previous PMTV experiments by showing that the interactions of BSMV TGB2 and TGB3 can be detected genetically in a yeast two-hybrid system and physically by affinity chromatography of TGB2 and TGB3 expressed in yeast, and we have mapped and identified the residues critical for these interactions (30). Moreover, our mutants demonstrated that interactions between TGB2 and TGB3 are essential for the cell-to-cell movement of the BSMV γb-GFP reporter virus (30). In the current work, we have extended these findings to show that the same site-specific mutations that interfere with the CW interactions of TGB2 and TGB3 also disrupt TGB3 targeting of TGB2 to the CW. We also have shown that TGB1 targeting to the wall is mediated by TGB2 and TGB3 interactions and that the most pronounced CW localization occurs when TGB2 and TGB3 are expressed in

ratios similar to those occurring during natural infections. Therefore, it appears that TGB2 has some role in TGB1 targeting even though we have been unable to detect direct physical interactions between the two proteins. TGB2 appears to function indirectly during TGB1 targeting by binding to TGB3 rather than to TGB1, and the fact that the TGB3 protein appears to be an order of magnitude lower in abundance than TGB2 and 100-fold lower in abundance than TGB1 suggests that movement involves the TGB3-mediated transport of large TGB1 and TGB2 complexes into and beyond the CW. Our recent characterization of TGB1 RNP complexes in infected tissue provides an example of the possible nature of such movement complexes (30).

We have previously applied several different approaches to demonstrate homologous TGB1 interactions and have mapped interactions of full-length proteins using site-specific mutations (30). These experiments indicate that helicase motifs I and II are critical for TGB1 interactions, so it was of interest to determine the subcellular localization of the mutant proteins. Interestingly, in the presence of TGB2 and TGB3, mutant M1 and M2 TGB1 proteins, both of which affect motif I residue 259, remained at the CW of plasmolyzed cells. However, the M3 mutation in motif II, which is also required for TGB1 binding interactions, and the M4, M5, and M7 mutants, which appear not to be required for interactions, were unable to form stable CW associations. Our interpretation of these results is that the ability to form homologous interactions per se is not a specific requirement for the CW targeting of TGB1 and that the M3, M4, M5, and M7 mutants are involved in functions other than those required for CW targeting. These functions may involve energy-dependent ATP binding and hydrolysis activities mediated by the helicase motif (13), and we are currently exploring these possibilities in more detail.

In sum, our current and previous studies (27, 30) are compatible with a model for BSMV movement and subcellular localization that depends on TGB protein interactions. In this context, it is worth noting that weak salt-sensitive single-stranded RNA binding activities were reported previously for the hordeivirus-like PMTV TGB2 protein (9), and these interactions suggest that hordeivirus-like TGB2 proteins might have an intermediate role in the transfer of newly synthesized viral RNAs to nascent TGB1 nucleoprotein complexes. We propose that such RNA binding and transfer interactions might occur at or within chloroplast-associated replication complexes, which have recently been shown to harbor small amounts of the TGB2 protein (53). TGB2 and TGB3 most likely form heterologous complexes during the coupled translation of sgRNAβ2 (60) on membrane-bound polysomes that may be in close proximity to the replicating complex. The TGB2-TGB3 complexes could then interact with TGB1 via TGB3 to facilitate the proximity required for interactions necessary for the transfer of TGB2-bound viral RNAs to nascent TGB1 RNP complexes. A large body of evidence supports a model whereby newly formed TGB1 RNP complexes are targeted to the PD by interactions between TGB2 and TGB3, although the cellular transport mechanisms resulting in such targeting are still a subject of some debate (18, 40, 47). However, there is a general consensus that the hordeivirus-like TGB3 proteins mediate RNP docking at the PD, and increasing evidence suggests that TGB2 and TGB3 both have the potential to mediate PD size exclusion limits (18, 40, 53). Although more direct experiments are needed to verify the mechanism of transit to adjacent cells, a plausible hypothesis is that the TGB2-TGB3 complex remains in the infected cells at the infection front during the delivery of viral nucleocapsids through the PD to adjacent cells and that both TGB proteins are targeted through the endocytic pathway for the recycling of additional rounds of transport or for degradation (19). Clearly, these scenarios raise a large number of unresolved questions, including the nature of the host interactions required to facilitate TGB protein and RNP transit as well as what series of events results in the conversion from the high levels of TGB1 expression noted at the leading edge of the infection boundary to the low levels of expression in cells close to the center of the infection focus (27). We are currently attempting to identify the hordeivirus-host interactions occurring during different phases of infection in order to provide a more comprehensive model of BSMV movement processes.

ACKNOWLEDGMENTS

We thank Nam-Hai Chua for the DsRed-talin plasmid and Pat Zambryski for plasmid pTMV-ROPL used for cloning of the P30-GFP PD marker. We also thank David Baulcombe for transgenic *N. benthamiana* seeds expressing GFP-KDEL.

This research was supported by U.S. Department of Agriculture competitive research grant 2008-35319-19225.

REFERENCES

1. **Bae, H., M. S. Kim, R. C. Sicher, H. J. Bae, and B. A. Bailey.** 2006. Necrosis- and ethylene-inducing peptide from Fusarium oxysporum induces a complex cascade of transcripts associated with signal transduction and cell death in Arabidopsis. Plant Physiol. **141:**1056–1067.
2. **Baulcombe, D. C.** 2004. RNA silencing in plants. Nature **431:**356–363.
3. **Bleykasten, C., D. Gilmer, H. Guilley, K. E. Richards, and G. Jonard.** 1996. Beet necrotic yellow vein virus 42 kDa triple gene block protein binds nucleic acid in vitro. J. Gen. Virol. **77:**889–897.
4. **Boevink, P., and K. J. Oparka.** 2005. Virus-host interactions during movement processes. Plant Physiol. **138:**1815–1821.
5. **Bragg, J. N., and A. O. Jackson.** 2004. The C-terminal region of the Barley stripe mosaic virus γb protein participates in homologous interactions and is required for suppression of RNA silencing. Mol. Plant Pathol. **5:**465–481.
6. **Bragg, J. N., H.-S. Lim, and A. O. Jackson.** 2008. Hordeiviruses, p. 459–467. *In* B. Mahy and M. van Regenmortel (ed.), Encyclopedia of virology, 3rd ed., vol. 2. Elsevier Ltd., Oxford, United Kingdom.
7. **Canto, T., and P. Palukaitis.** 2005. Subcellular distribution of mutant movement proteins of *Cucumber mosaic virus* fused to green fluorescent proteins. J. Gen. Virol. **86:**1223–1228.
8. **Citovsky, V., D. Knorr, G. Schuster, and P. Zambryski.** 1990. The P30 movement protein of tobacco mosaic virus is a single-stranded nucleic acid binding protein. Cell **60:**637–647.
9. **Cowan, G. H., F. Lioliopoulou, A. Ziegle, and L. Torrance.** 2002. Subcellular localization, protein interactions, and RNA binding of Potato mop-top virus triple gene block proteins. Virology **298:**106–115.
10. **Crawford, K. M., and P. C. Zambryski.** 2001. Non-targeted and targeted protein movement through plasmodesmata in leaves in different developmental and physiological states. Plant Physiol. **125:**1802–1812.
11. **Deng, M., J. N. Bragg, S. Ruzin, D. Schichnes, D. King, M. M. Goodin, and A. O. Jackson.** 2007. Role of the sonchus yellow net virus N protein in formation of nuclear viroplasms. J. Virol. **81:**5362–5374.
12. **Ding, B., J. S. Haudenshield, R. J. Hull, S. Wolf, R. N. Beachy, and W. J. Lucas.** 1992. Secondary plasmodesmata are specific sites of localization of the tobacco mosaic virus movement protein in transgenic tobacco plants. Plant Cell **4:**915–928.
13. **Donald, R. G., D. M. Lawrence, and A. O. Jackson.** 1997. The barley stripe mosaic virus 58-kilodalton βb protein is a multifunctional RNA binding protein. J. Virol. **71:**1538–1546.
14. **Donald, R. G., H. Zhou, and A. O. Jackson.** 1993. Serological analysis of barley stripe mosaic virus-encoded proteins in infected barley. Virology **195:**659–668.
15. **Erhardt, M., M. Morant, C. Ritzenthaler, C. Stussi-Garaud, H. Guilley, K. E. Richards, G. Jonard, S. Bouzoubaa, and D. Gilmer.** 2000. P42 movement protein of beet necrotic yellow vein virus is targeted by the movement proteins p13 and p15 to punctate bodies associated with plasmodesmata. Mol. Plant-Microbe Interact. **13:**520–528.

16. **Goodin, M. M., R. G. Dietzgen, D. Schichnes, S. Ruzin, and A. O. Jackson.** 2002. pGD vectors: versatile tools for the expression of green and red fluorescent protein fusions in agroinfiltrated plant leaves. Plant J. **3:**375–383.
17. **Gorshkova, E. N., T. N. Erokhina, T. A. Stroganova, N. E. Yelina, A. A. Zamyatnin, Jr., N. O. Kalinina, J. Schiemann, A. G. Solovyev, and S. Y. Morozov.** 2003. Immunodetection and fluorescent microscopy of transgenically expressed hordeivirus TGBp3 movement protein reveals its association with endoplasmic reticulum elements in close proximity to plasmodesmata. J. Gen. Virol. **84:**985–994.
18. **Haupt, S., G. H. Cowan, A. Ziegler, A. G. Roberts, K. J. Oparka, and L. Torrance.** 2005. Two plant-viral movement proteins traffic in the endocytic recycling pathway. Plant Cell **17:**164–181.
19. **Jackson, A. O., H.-S. Lim, J. N. Bragg, U. Ganesan, and M. Y. Lee.** 2009. Hordeivirus replication, movement and pathogenesis. Annu. Rev. Phytopathol. **47:**385–422.
20. **Johansen, L. K., and J. C. Carrington.** 2001. Silencing on the spot. Induction and suppression of RNA silencing in the Agrobacterium-mediated transient expression system. Plant Physiol. **126:**930–938.
21. **Ju, H. J., T. D. Samuels, Y. S. Wang, E. Blancaflor, M. Payton, R. Mitra, K. Krishnamurthy, R.S. Nelson, and J. J. Verchot-Lubicz.** 2005. The Potato virus X TGBp2 movement protein associates with endoplasmic reticulum-derived vesicles during virus infection. Plant Physiol. **138:**1877–1895.
22. **Kalinina, N. O., D. V. Rakitina, A. G. Solovyev, J. Schiemann, and S. Y. Morozov.** 2002. RNA helicase activity of the plant virus movement proteins encoded by the first gene of the triple gene block. Virology **296:**321–329.
23. **Kalinina, N. O., D. A. Rakitina, N. E. Yelina, A. A. Zamyatnin, T. A. Stroganova, D. V. Klinov, V. V. Prokhorov, S. V. Ustinova, B. K. Chernov, J. Schiemann, A. G. Solovyev, and S. Y. Morozov.** 2001. RNA binding properties of the 63-kDa protein encoded by triple gene block of poa semilatent hordeivirus. J. Gen. Virol. **82:**2569–2578.
24. **Kawakami, S., Y. Watanabe, and R. N. Beachy.** 2004. Tobacco mosaic virus infection spreads cell to cell as intact replication complexes. Proc. Natl. Acad. Sci. USA **101:**6291–6296.
25. **Kost, B., P. Spielhofer, and N. H. Chua.** 1998. A GFP-mouse talin fusion protein labels plant actin filaments in vivo and visualizes the actin cytoskeleton in growing pollen tubes. Plant J. **16:**393–401.
26. **Krishnamurthy, K., M. Heppler, R. Mitra, E. Blancaflor, M. Payton, R. S. Nelson, and J. Verchot-Lubicz.** 2003. The Potato virus X TGBp3 protein associates with the ER network for virus cell-to-cell movement. Virology **309:**135–151.
27. **Lawrence, D. M., and A. O. Jackson.** 2001. Interactions of the TGB1 protein during cell-to-cell movement of *Barley stripe mosaic virus*. J. Virol. **75:**8712–8723.
28. **Lawrence, D. M., and A. O. Jackson.** 2001. Requirements for cell-to-cell movement of Barley stripe mosaic virus in monocot and dicot hosts. Mol. Plant Pathol. **2:**65–75.
29. **Leshchiner, A. D., A. G. Solovyev, S. Y. Morozov, and N. O. Kalinina.** 2006. A minimal region in the NTPase/helicase domain of the TGBp1 plant virus movement protein is responsible for ATPase activity and cooperative RNA binding. J. Gen. Virol. **87:**3087–3095.
30. **Lim, H.-S., J. N. Bragg, U. Ganesan, D. M. Lawrence, J. Yu, M. Isogai, J. Hammond, and A. O. Jackson.** 2008. Triple gene block protein interactions involved in movement of *Barley stripe mosaic virus*. J. Virol. **82:**4991–5006.
31. **Lin, N.-S., and W. G. Langenberg.** 1985. Distribution of barley stripe mosaic virus protein in infected wheat root and shoot tips. J. Gen. Virol. **65:**2217–2224.
32. **Lin, N.-S., and W. G. Langenberg.** 1984. Chronology of appearance of barley stripe mosaic virus protein in infected wheat cells. J. Ultrastruct. Res. **89:**309–323.
33. **Liou, D. Y., Y. H. Hsu, C. H. Wung, W. H. Wang, N. S. Lin, and B. Y. Chang.** 2000. Functional analyses and identification of two arginine residues essential to the ATP-utilizing activity of the triple gene block protein 1 of bamboo mosaic potexvirus. Virology **277:**336–344.
34. **Livak, K. J., and T. D. Schmittgen.** 2001. Analysis of relative gene expression data using real-time quantitative PCR and the $2^{-\Delta\Delta CT}$ method. Methods **25:**402–408.
35. **Lough, T. J., K. Shash, B. Xoconostle-Cazares, K. R. Hofstra, D. L. Beck, E. Balmori, R. L. Forster, and W. J. Lucas.** 1998. Molecular dissection of the mechanism by which potexvirus triple gene block proteins mediate cell-to-cell transport of infectious RNA. Mol. Plant-Microbe Interact. **11:**801–814.
36. **Lucas, W. J.** 2006. Plant viral movement proteins: agents for cell-to-cell trafficking of viral genomes. Virology **344:**169–184.
37. **Lucas, W. J., and J. Y. Lee.** 2004. Plasmodesmata as a supracellular control network in plants. Nat. Rev. Mol. Cell Biol. **5:**712–726.
38. **Mitra, R., K. Krishnamurthy, E. Blancaflor, M. Payton, R. S. Nelson, and J. Verchot-Lubicz.** 2003. The Potato virus X TGBp2 protein association with the endoplasmic reticulum plays a role in but is not sufficient for viral cell-to-cell movement. Virology **312:**35–48.
39. **Morozov, S. Y., and A. G. Solovyev.** 2003. Triple gene block: modular design of a multifunctional machine for plant virus movement. J. Gen. Virol. **84:**1351–1366.
40. **Oparka, K. J.** 2004. Getting the message across: how do plant cells exchange macromolecular complexes? Trends Plant Sci. **9:**33–41.
41. **Petty, I. T., R. French, R. W. Jones, and A. O. Jackson.** 1990. Identification of barley stripe mosaic virus genes involved in viral RNA replication and systemic movement. EMBO J. **9:**3453–3457.
42. **Petty, I. T., B. G. Hunter, N. Wei, and A. O. Jackson.** 1989. Infectious barley stripe mosaic virus RNA transcribed from full-length genomic cDNA clones. Virology **171:**342–349.
43. **Petty, I. T., B. G. Hunter, and A. O. Jackson.** 1988. A novel strategy for one-step cloning of full-length cDNA and its application to the genome of barley stripe mosaic virus. Gene **74:**423–432.
44. **Rouleau, M., R. J. Smith, J. B. Bancroft, and G. A. Mackie.** 1994. Purification, properties, and subcellular localization of foxtailmosaic potexvirus 26-kDa protein. Virology **204:**254–265.
45. **Samuels, T. D., H. J. Ju, C. M. Ye, C. M. Motes, E. B. Blancaflor, and J. Verchot-Lubicz.** 2007. Subcellular targeting and interactions among the Potato virus X TGB proteins. Virology **367:**375–389.
46. **Schepetilnikov, M. V., U. Manske, A. G. Solovyev, A. A. Zamyatnin, Jr., J. Schiemann, and S. Y. Morozov.** 2005. The hydrophobic segment of Potato virus X TGBp3 is a major determinant of the protein intracellular trafficking. J. Gen. Virol. **86:**2379–2391.
47. **Schepetilnikov, M. V., A. G. Solovyev, E. N. Gorshkova, J. Schiemann, A. I. Prokhnevsky, V. Dolja, and S. Y. Morozov.** 2008. Intracellular targeting of a hordeiviral membrane-spanning movement protein: sequence requirements and involvement of an unconventional mechanism. J. Virol. **82:**1284–1293.
48. **Scholthof, H. B.** 2005. Plant virus transport: motions of functional equivalence. Trends Plant Sci. **10:**376–382.
49. **Solovyev, A. G., E. I. Savenkov, A. A. Agranovsky, and S. Y. Morozov.** 1996. Comparisons of the genomic cis-elements and coding regions in RNA beta components of the hordeiviruses barley stripe mosaic virus, lychnis ringspot virus, and poa semilatent virus. Virology **219:**9–18.
50. **Solovyev, A. G., T. A. Stroganova, A. A. Zamyatnin, O. N. Fedorkin, J. Schiemann, and S. Y. Morozov.** 2000. Subcellular sorting of small membrane-associated triple gene block proteins: TGBp3-assisted targeting of TGBp2. Virology **269:**113–127.
51. **Tamai, A., and T. Meshi.** 2001. Cell-to-cell movement of potato virus X: the role of p12 and p8 encoded by the second and third open reading frames of the triple gene block. Mol. Plant-Microbe Interact. **14:**1158–1167.
52. **Tomenius, K., D. Clapham, and T. Meshi.** 1987. Localization by immunogold cytochemistry of the virus-coded 30k protein in plasmodesmata of leaves infected with tobacco mosaic virus. Virology **160:**363–371.
53. **Torrance, L., G. H. Cowan, T. Gillespie, A. Ziegler, and C. Lacomme.** 2006. Barley stripe mosaic virus-encoded proteins triple-gene block 2 and γb localize to chloroplasts in virus-infected monocot and dicot plants, revealing hitherto-unknown roles in virus replication. J. Gen. Virol. **87:**2403–2411.
54. **Verchot-Lubicz, J.** 2005. A new cell-to-cell transport model for potexviruses. Mol. Plant-Microbe Interact. **18:**283–290.
55. **Waigmann, E., S. Ueki, K. Trutnyeva, and V. Citovsky.** 2004. The ins and outs of non-destructive cell-to-cell and systemic movement of plant viruses. Crit. Rev. Plant Sci. **23:**195–250.
56. **Wung, C. H., Y. H. Hsu, D. Y. Liou, W. C. Huang, N. S. Lin, and B. Y. Chang.** 1999. Identification of the RNA-binding sites of the triple gene block protein 1 of bamboo mosaic potexvirus. J. Gen. Virol. **80:**1119–1126.
57. **Wurch, T., F. Lestienne, and P. Pauwels.** 1998. A modified overlap extension PCR method to create chimeric genes in the absence of restriction enzymes. Biotechnol. Tech. **12:**653–657.
58. **Zamyatnin, A. A., A. G. Solovyev, E. I. Savenkov, A. Germudson, M. Sandgren, J. P. T. Valkonen, and S. Y. Morozov.** 2004. Transient coexpression of individual genes encoded by the triple gene block of potato mop-top virus reveals requirements for TGBp1 trafficking. Mol. Plant-Microbe Interact. **17:**921–930.
59. **Zamyatnin, A. A., A. G. Solovyev, A. A. Sablina, A. A. Agranovsky, L. Katul, H. J. Vetten, J. Schiemann, A. E. Hinkkanen, K. Lehto, and S. Y. Morozov.** 2002. Dual-colour imaging of membrane protein targeting directed by poa semilatent virus movement protein TGBp3 in plant and mammalian cells. J. Gen. Virol. **83:**651–662.
60. **Zhou, H., and A. O. Jackson.** 1996. Expression of the barley stripe mosaic virus RNA β "triple gene block." Virology **216:**367–379.